

DOI:10.1002/ejic.201402378

## BOX Ligands in Biomimetic Copper-Mediated Dioxygen Activation: A Hemocyanin Model

Adam Walli,<sup>[a]</sup> Sebastian Dechert,<sup>[a]</sup> Matthias Bauer,<sup>[b]</sup>  
Serhiy Demeshko,<sup>[a]</sup> and Franc Meyer\*<sup>[a]</sup>



**Keywords:** Bioinorganic chemistry / Copper / Enzyme catalysis / O-O activation / Peroxo complexes

The  $\mu$ - $\eta^2$ : $\eta^2$ -peroxodicopper(II) core found in the oxy forms of the active sites of type III dicopper proteins have been a key target for bioinorganic model studies. Here, it is shown that simple bis(oxazolines) (BOXs), which are classified among the so-called “privileged ligands”, provide a suitable scaffold for supporting such biomimetic copper/dioxygen chemistry. Three derivatives  $R^tH$ BOX-Me<sub>2</sub> (R = H, Me, *t*Bu) with different backbone substituents have been used. Their bis(oxazoline)-copper(I) complexes bind dioxygen to yield biomimetic  $\mu$ - $\eta^2$ : $\eta^2$ -peroxodicopper(II) species. O<sub>2</sub> can be reversibly released upon an increase in temperature. Their formation kinetics have been studied under cryo-stopped-flow conditions for the *t*Bu derivative, giving activation parameters  $\Delta H^\ddagger_{\text{on}} = (2.27 \pm 0.18)$  kcal mol<sup>-1</sup>,  $\Delta S^\ddagger_{\text{on}} = (-46.3 \pm 0.8)$  cal K<sup>-1</sup> mol<sup>-1</sup> for the binding event and  $\Delta H^\ddagger_{\text{off}} = (11.7 \pm 1.9)$  kcal mol<sup>-1</sup>,  $\Delta S^\ddagger_{\text{off}} = (-16.1 \pm 8.2)$  cal K<sup>-1</sup> mol<sup>-1</sup> for the release of O<sub>2</sub>, as well as thermodynamic parameters  $\Delta H^\circ = (-10.0 \pm 1.7)$  kcal mol<sup>-1</sup> and  $\Delta S^\circ = (-32.7 \pm 7.4)$  cal K<sup>-1</sup> mol<sup>-1</sup> for this equilibrium. The  $\mu$ - $\eta^2$ : $\eta^2$ -peroxodicopper(II) complexes have been isolated as surprisingly stable solids and investigated in depth by a variety of methods, both

in solution and in the solid state. Resonance Raman spectroscopy revealed a characteristic isotope-sensitive stretch  $\tilde{\nu}_{\text{O-O}} = 731\text{--}742$  cm<sup>-1</sup> ( $\Delta[^{18}\text{O}_2] \approx -39$  cm<sup>-1</sup>) and an intense feature around 280 cm<sup>-1</sup> diagnostic for the fundamental symmetric Cu<sub>2</sub>O<sub>2</sub> core vibration. A slight butterfly-shape of the Cu<sub>2</sub>O<sub>2</sub> core has been derived from EXAFS data and DFT calculations. SQUID magnetic data evidenced strong antiferromagnetic coupled Cu<sup>II</sup><sub>2</sub> ( $-2J \geq 1000$  cm<sup>-1</sup>). Thermal degradation in solution yields bis(hydroxo)-bridged[(<sup>t</sup>Bu,<sup>H</sup>BOX-Me<sub>2</sub>)(L)-Cu(OH)]<sub>2</sub>(PF<sub>6</sub>)<sub>2</sub> (L = H<sub>2</sub>O, MeCN or THF); whereas in the case of <sup>H</sup>,<sup>H</sup>BOX-Me<sub>2</sub>, ligand oxygenation has been detected. Preliminary reactivity studies with the substrate 2,4-di-*tert*-butylphenol indicate the formation of the C–C coupling product 3,3',5,5'-tetra-*tert*-butyl-2,2'-biphenol, whereas *ortho*-hydroxylation was not observed. The copper(I) complex [(<sup>t</sup>Bu,<sup>H</sup>BOX-Me<sub>2</sub>)Cu(MeCN)]PF<sub>6</sub> as well as two dicopper(II) complexes [(L)(<sup>t</sup>Bu,<sup>H</sup>BOX-Me<sub>2</sub>)Cu(OH)]<sub>2</sub>(PF<sub>6</sub>)<sub>2</sub> have been characterised by single-crystal X-ray diffraction. Considering the vast number of known BOX derivatives, a rich and versatile Cu/O<sub>2</sub> chemistry based on this platform is anticipated.

### Introduction

Copper-dioxygen adducts have attracted much interest during the last two decades because of their biological relevance and their promising prospects for bioinspired oxidation and oxygenation catalysis.<sup>[1–4]</sup> Type III copper proteins such as the O<sub>2</sub>-transporter hemocyanin<sup>[5,6]</sup> and the related enzymes tyrosinase<sup>[7,8]</sup> and catechol oxidase<sup>[9]</sup> contain, in their oxy form, a side-on  $\mu$ - $\eta^2$ : $\eta^2$ -peroxodicopper(II) core that results from O<sub>2</sub>-binding to the dicopper(I) deoxy state (Figure 1).<sup>[4,10,11]</sup> A number of synthetic analogue complexes featuring the  $\mu$ - $\eta^2$ : $\eta^2$ -peroxo unit (see also Table S1 in the Supporting Information), as well as other related

Cu<sub>2</sub>O<sub>2</sub> motifs, have also been prepared.<sup>[1,12–16]</sup> Most of them are quite unstable even at low temperatures, whereas others show reversible O<sub>2</sub>-binding related to hemocyanin.<sup>[17–19]</sup> The particular Cu<sub>2</sub>O<sub>2</sub> structure obtained depends on the precise nature of the capping ligands, inter alia on their denticity and steric demand, and on the types of counterion or solvent.<sup>[1]</sup> Subtleties of the electronic structures of such Cu<sub>2</sub>O<sub>2</sub> cores have been studied in detail and have been found to critically determine their spectroscopic properties and reactivity.<sup>[1,2,10,20–24]</sup> Hence, there is continuous interest in new and tuneable ligands and their respective copper complexes that might support biomimetic copper-dioxygen chemistry, and that might advance our understanding of the delicate subtleties of copper–dioxygen interactions.

Bis(oxazoline) derivatives (BOXs) are classified among the so-called “privileged ligands” and have found widespread applications,<sup>[27–34]</sup> but surprisingly have not been explored in copper-mediated O<sub>2</sub> activation until now. Having recently developed some new BOX derivatives,<sup>[35]</sup> we report here a detailed investigation on the reversible O<sub>2</sub> binding by

[a] Institut für Anorganische Chemie, Georg-August-Universität Göttingen, Germany  
Tammannstr. 4, 37077 Göttingen  
E-mail: franc.meyer@chemie.uni-goettingen.de  
<http://www.meyer.chemie.uni-goettingen.de/>

[b] Department of Chemistry, University of Paderborn, Warburger Str. 100, 33098 Paderborn, Germany

Supporting information for this article is available on the WWW under <http://dx.doi.org/10.1002/ejic.201402378>.

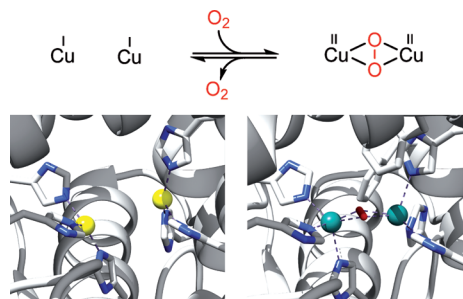
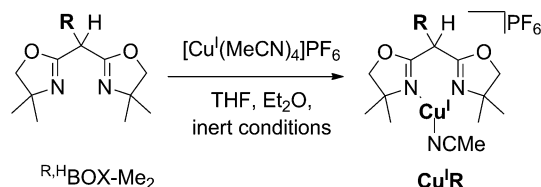
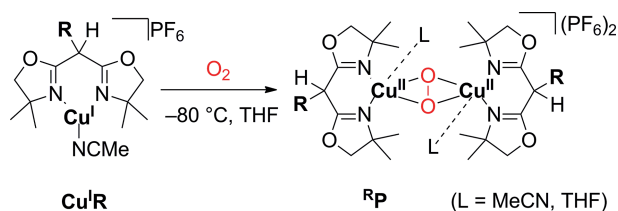


Figure 1. (Top) Schematic drawing of  $O_2$  binding to give the  $\mu$ - $\eta^2$ : $\eta^2$ -peroxodicopper(II) core. (Bottom) View of the active site of the 73 kDa arthropod subunit II hemocyanin (Hc) of the Atlantic horseshoe crab, *Limulus polyphemus*, determined by X-ray diffraction. Deoxy-Hc (left) at 2.2 Å resolution (PDB ID: 1LLA),<sup>[25]</sup> Cu...Cu distance: 4.61 Å; Oxy-Hc [right,  $\mu$ - $\eta^2$ : $\eta^2$ -peroxodicopper(II)] at 2.4 Å resolution (PDB ID: 1OXY),<sup>[26]</sup> distances [Å]: Cu...Cu: 3.59, O–O: 1.41, Cu–N<sub>eq</sub>: 2.1, Cu–N<sub>ax</sub>: 2.4. Colour code: white, protein backbone; blue, nitrogen; red, oxygen; yellow, copper(I); teal, copper(II).

copper(I) complexes of the three ligands  $R^H$ BOX-Me<sub>2</sub> (R = H, Me, *t*Bu; Scheme 1 and Scheme 2) and on the resulting dicopper–peroxo complexes.



Scheme 1. Preparation of copper(I)-bis(oxazoline) complexes  $Cu^I R$  (R = *t*Bu, Me, H).



Scheme 2. Activation of dioxygen with copper(I)-bis(oxazoline) complexes  $Cu^I R$  (R = *t*Bu, Me, H) to form  $\mu$ - $\eta^2$ : $\eta^2$ -peroxodicopper(II) complexes  $^R P$ .

## Results and Discussion

### Copper(I) Complexes of BOXs

Reactions of the three ligands  $R^H$ BOX-Me<sub>2</sub> (R = *t*Bu, Me, H) with  $[Cu(MeCN)_4]PF_6$  (Scheme 1) in tetrahydrofuran (THF) and other solvents give the air-sensitive copper(I) complexes  $[(R^H BOX-Me_2)Cu(MeCN)]PF_6$  ( $Cu^I R$ ) as colourless solutions. For further reactions, the complexes were generally not isolated, but their solutions were used in situ. However, to establish their identity,  $Cu^I tBu$  and  $Cu^I H$  have been isolated and characterised, and the molecular structure of  $Cu^I tBu$  was ascertained by X-ray

diffraction analysis of a colourless single crystal obtained from THF/Et<sub>2</sub>O solution under inert conditions (Figure 2, Table 1). The copper ion is coordinated in a trigonal planar fashion by the  $tBu^H$ BOX-Me<sub>2</sub> ligand with a bite angle N–Cu–N of 93.6° and by an exogenous MeCN solvent molecule. The BOX ligand adopts a boat-shaped coordination geometry. Owing to the steric bulk of the *t*Bu group, the angle between this residue and the {N<sub>3</sub>Cu} coordination plane is quite large (ca. 80°). NMR analysis of  $Cu^I tBu$  and  $Cu^I H$  is in agreement with the solid-state structure being maintained in solution. Cyclic voltammetry of a MeCN solution of  $Cu^I tBu$  (see the Supporting Information and Figures S1 and S2 for details) shows a quasi-reversible electrochemical process with anodic peak potential  $E_{pa} = 0.63$  V vs. SCE, assigned to the  $Cu^I \rightarrow Cu^{II} + e^-$  oxidation. Large separation of the anodic and cathodic peak potentials ( $\Delta E_p = 0.30$  V) for this couple on the cyclic voltammetry time-scale is common for copper complexes because of substantial structural rearrangements upon shuttling between  $Cu^I$  and  $Cu^{II}$ , which favour very different coordination geometries.

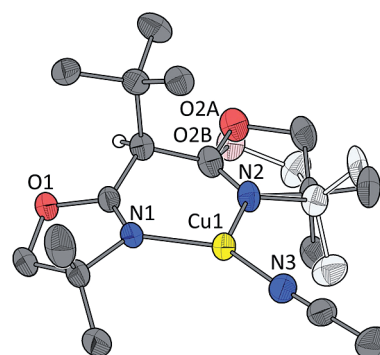


Figure 2. X-ray solid-state molecular structure of  $Cu^I tBu$ . ORTEP plot with significant atoms labelled. Displacement ellipsoids are drawn at the 50% probability level; most hydrogen atoms have been omitted for clarity; atoms located at a second site (B) due to crystallographic disorder are drawn in lighter shade. See Figure S18 for van-der-Waals representations. Significant interatomic distances and angles are listed in Table 1.

Table 1. Significant geometric information of the solid-state structure of  $Cu^I tBu$  in Figure 2. Interatomic distances [Å] and angles [°].

Atoms 1,2	<i>d</i> 1,2 / Å	Atoms 1,2,3	Angle 1,2,3
Cu1–N1	1.9630(17)	N1–Cu1–N2	93.56(7)
Cu1–N2	2.0037(18)	N3–Cu1–N1	142.62(8)
Cu1–N3	1.8649(19)	N3–Cu1–N2	123.64(8)
N3–C16	1.131(3)	Cu1–N3–C16	175.0(2)

### Activation of Dioxygen

Oxygenation of the colourless copper(I) complexes  $Cu^I R$  at  $-78$  °C in THF affords violet to purple  $\mu$ - $\eta^2$ : $\eta^2$ -peroxodicopper(II) complexes  $^R P$  (Scheme 2) with intense optical absorption bands at 333 nm ( $\epsilon = 48.0 \pm 1.1$  mm<sup>−1</sup> cm<sup>−1</sup>) and

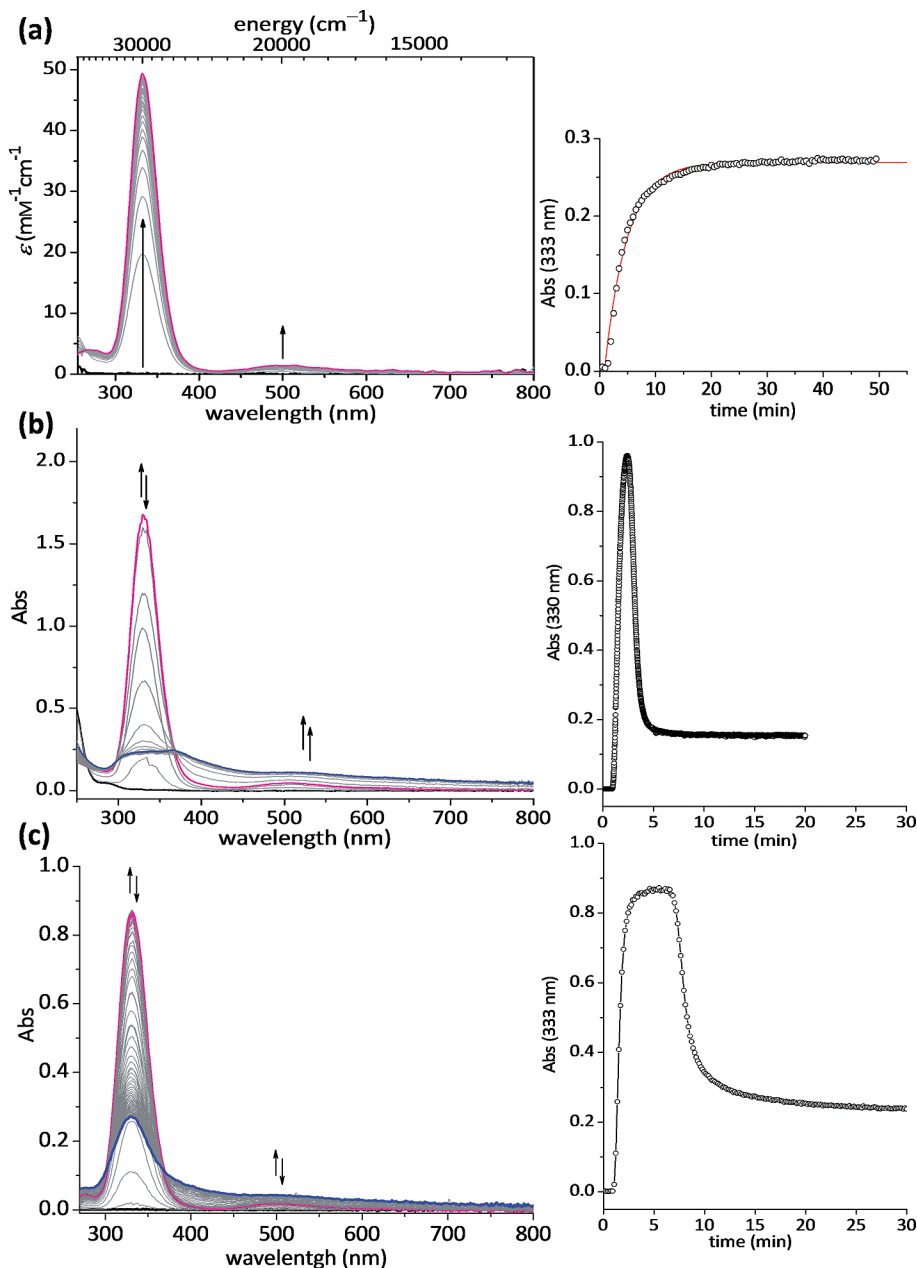


Figure 3. UV/Vis spectra and formation of  $\mu\text{-}\eta^2\text{:}\eta^2\text{-peroxo complexes}^{\text{RP}}$  (left side, magenta lines), obtained upon oxygenation of  $\text{Cu}^{\text{I}}\text{R}$  (black lines) in THF at  $-78\text{ }^{\circ}\text{C}$ . R = (a) *t*Bu, (b) H, and (c) Me. Final spectra after precipitation of peroxo complexes (blue lines, R = H, Me). Concentrations of  $\text{Cu}^{\text{I}}\text{R}$  were 0.30 mM (R = *t*Bu), 1.13 mM (R = H) and 0.79 mM (R = Me). Kinetic traces at 333 nm (right side, circles); traces were obtained from an additional measurement (R = H) or from a cryo-stopped-flow experiment (R = *t*Bu, with kinetic first-order-rate fit, red line). See Table 2 for rate constants of formation and spectroscopic parameters.

500 nm ( $2.1 \pm 0.2\text{ mM}^{-1}\text{ cm}^{-1}$ ) in the case of  ${}^t\text{BuP}$  and nearly identical features in the case of  $\text{HP}$  and  $\text{MeP}$  (Figure 3, Table 2). The oxygenation could be achieved either by the injection of  $\text{O}_2$  gas into solutions of  $\text{Cu}^{\text{I}}\text{R}$  in THF (at  $-78\text{ }^{\circ}\text{C}$  under Ar or  $\text{N}_2$  atmosphere) or by the slow injection of the  $\text{Cu}^{\text{I}}\text{R}/\text{THF}$  solutions into  $\text{O}_2$ -saturated THF at  $-78\text{ }^{\circ}\text{C}$ .

The optical features are archetypical for a  $\mu\text{-}\eta^2\text{:}\eta^2\text{-peroxo-dicopper(II)}$  species and are closely analogous to the spectroscopic features of oxyhemocyanine and oxytyrosinase. Prominent bands have previously been ascribed to

$\pi_{\sigma}^* \rightarrow d_{x^2-y^2}$  (in-plane) and  $\pi_{\nu}^* \rightarrow d_{x^2-y^2}$  (out-of-plane)  $\text{Cu}^{\text{II}} \leftarrow \text{O}_{\text{peroxo}}$  ligand-to-metal charge transfer (LMCT) transitions, the former being more intense due to a better overlap of orbitals.<sup>[22,36]</sup> Although similar to absorptions of previously reported systems, with  $\lambda_{\text{max}}$  ( $\epsilon, \text{mM}^{-1}\text{ cm}^{-1}$ ) = ca. 340–380 nm (ca. 18–25) and ca. 510–550 nm (ca. 1),<sup>[1]</sup> both CT bands of  ${}^{\text{RP}}$  are at relatively high energy compared to known systems and are remarkably more intense (indicated also by a Beer's law plot for  ${}^t\text{BuP}$ , see Figure S4). The strong 333 nm transition for  ${}^t\text{BuP}$  ( $\epsilon = 48\text{ mM}^{-1}\text{ cm}^{-1}$ ) is only comparable to model complexes with ethylene diamine de-

Table 2. Spectroscopic features and kinetic data of  $\mu$ - $\eta^2$ : $\eta^2$ -peroxodicopper(II) complexes <sup>R</sup>P.

	Solvent	UV/Vis: $\lambda_{\max}$ [nm] ( $\epsilon$ [mm <sup>-1</sup> cm <sup>-1</sup> ]) <sup>[a]</sup>	RR: $\tilde{\nu}$ [cm <sup>-1</sup> ] ( $\Delta$ [ <sup>18</sup> O <sub>2</sub> ]) <sup>[b]</sup>		$k_{\text{obs}}$ <sup>[c]</sup> [min <sup>-1</sup> ]
			Cu–Cu	O–O	
<sup>t</sup> BuP	THF	333 (48.0), 509 (2.1)	278	729	0.25
	acetone	334 (47), 496 (1.1)			0.23
<sup>H</sup> P	solid	263, 334, 520, ~620 (sh)	279 (1)	731 (39)	
	THF	330 (> 30), 504 (> 0.8) <sup>[d]</sup>			> 1
<sup>M</sup> eP	solid	271, 332, 512, ~620 (sh)	282 (0)	742 (39)	
	THF	333 (> 22), 496 (> 0.5) <sup>[d]</sup>			~ 1.5
<sup>M</sup> eP	solid	261, 331, 493, 600 <sup>[e]</sup>	282	735	

[a] Solutions at  $-78$  °C, solids (diffuse reflectance) at room temp., sh = shoulder. [b] Resonance Raman spectra of solutions at  $-60$  °C, solids at room temp. [c] Formation upon O<sub>2</sub> injection at  $-78$  °C. [d] Low solubility. [e] Partly decomposed.

rived ligand systems (ca. 34–40 mm<sup>-1</sup> cm<sup>-1</sup>). Dicopper–peroxo complexes of those bidentate ligands usually feature undefined weak axial solvent or counterion ligation; intimate interaction with the counteranion was observed spectroscopically.<sup>[37–39]</sup> This suggested the presence of weakly bound axial solvent ligands also in <sup>R</sup>P, which is consistent with EXAFS data (see below).

The reactions of all three Cu<sup>I</sup>R with O<sub>2</sub> were found to follow first-order kinetics under the applied conditions, and the traces of the ~ 333 and ~ 500 nm features could be fitted with single exponential functions to obtain rate constants  $k_{\text{obs}}$  (Table 2). The rate constants were found to increase with reduced steric demand of the backbone residue R. The formation kinetics were investigated more closely with Cu<sup>I</sup>tBu (see below). Whereas <sup>t</sup>BuP is both, soluble in THF and sufficiently stable at low temperatures for an extended time, the solubilities of <sup>H</sup>P and <sup>M</sup>eP were rather limited and they were found to precipitate from their solutions during the oxygenation reaction (Figure 3). Although the relatively limited solubility of all three complexes is problematic to analysis and experiments in solution, it is advantageous for isolation of the peroxo complexes as solids (see below). The UV/Vis bands of <sup>t</sup>BuP are similar in acetone and in THF solutions (Table 2, Figure S6a), whereas no peroxo complex formation was observable in CH<sub>2</sub>Cl<sub>2</sub>.

<sup>R</sup>P are thermolabile at temperatures above approximately  $-60$  °C. The oxygenation reaction of <sup>t</sup>BuP was found to be reversible in THF (Figure S5): warming to  $-15$  °C under inert gas, followed by recooling and admitting O<sub>2</sub>, allowed sequential cycles of O<sub>2</sub> binding and release. The half-life  $t_{1/2}$  of <sup>t</sup>BuP upon warming to  $-15$  °C was around 3 min. Applying vacuum to a solution of <sup>t</sup>BuP in acetone induces O<sub>2</sub> release already at  $-78$  °C; however, slow decomposition of <sup>t</sup>BuP was evident in acetone (Figure S6).

In  $\mu$ - $\eta^2$ : $\eta^2$ -peroxodicopper(II) complexes, the O–O bond is significantly weakened compared with H<sub>2</sub>O<sub>2</sub> ( $\tilde{\nu}_{\text{O–O}} = 880$  cm<sup>-1</sup>) due to backbonding; known systems have characteristic resonance Raman (RR) frequencies and isotope shifts of  $\tilde{\nu}_{\text{O–O}} = 730$ – $760$  cm<sup>-1</sup> ( $\Delta$ [<sup>18</sup>O<sub>2</sub>] ca. 40 cm<sup>-1</sup>). In contrast, 1,2-*trans*-peroxo, 1,2-*cis*-peroxo,<sup>[40]</sup> and bis( $\mu$ -oxo) dicopper systems have  $\tilde{\nu}_{\text{O–O}} \approx 830$  cm<sup>-1</sup> (46),  $\tilde{\nu}_{\text{O–O}} \approx 800$  cm<sup>-1</sup> (45) and  $\tilde{\nu}_{\text{Cu–O}} \approx 600$  cm<sup>-1</sup> (28), respectively.<sup>[1]</sup> RR spec-

troscopy ( $\lambda_{\text{ex}} = 632.8$  nm) of a solution of <sup>t</sup>BuP in THF showed a Raman shift of 729 cm<sup>-1</sup> (Figure 4), typical for the weak  $\nu(\text{O–O})$  stretch of the  $\mu$ - $\eta^2$ : $\eta^2$ -bound peroxide. An intense feature at 278 cm<sup>-1</sup> is also diagnostic for this side-on peroxo complex and has been assigned as the fundamental symmetric Cu<sub>2</sub>O<sub>2</sub> core vibration,  $\nu(\text{Cu–Cu})$ .<sup>[41]</sup> Additional RR spectra are discussed below; no <sup>18</sup>O isotopic substitution is provided for samples in solution due to problematic solubility and weak intensity.

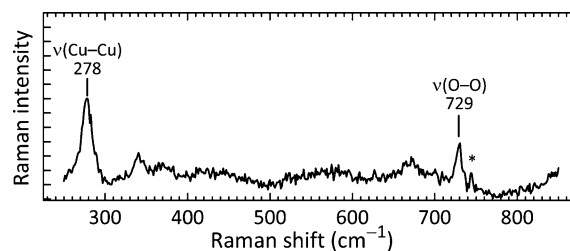
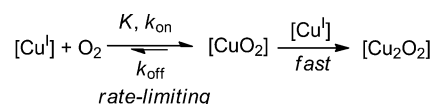


Figure 4. Resonance Raman (RR) spectrum of <sup>t</sup>BuP ( $\lambda_{\text{ex}} = 632.8$  nm) in THF solution at 213 K. The asterisk at 745 cm<sup>-1</sup> indicates PF<sub>6</sub><sup>-</sup>.

### Cryo-Stopped-Flow Kinetic Measurements

The kinetics of O<sub>2</sub> activation by Cu<sup>I</sup>tBu were studied by using stopped-flow-UV/Vis techniques under cryo conditions (see Experimental section and the Supporting Information for details). Analysis of all recorded UV/Vis spectra, from stopped-flow and other experiments, showed no detectable accumulation of intermediates. This suggests the following mechanism, as likewise found in related complexes:<sup>[2]</sup>



Here, the initially formed CuO<sub>2</sub> complex is instantly trapped by a second Cu<sup>I</sup>tBu molecule and the first step is the rate-determining step. With an excess of O<sub>2</sub> present, this reaction follows pseudo-first-order conditions:<sup>[42,43]</sup>

$$k_{\text{obs}} = k_{\text{on}}[\text{O}_2] + k_{\text{off}}$$

Variation of the O<sub>2</sub> concentration led to a second-order rate constant  $k_{\text{on}}$  for O<sub>2</sub> binding and a first-order constant  $k_{\text{off}}$  for the release, from the plot of  $k_{\text{obs}}$  vs. O<sub>2</sub> concentration (Figure 5, Table 3). The plot shows a linear relationship with a relatively large  $y$ -intercept above  $-60$  °C. Such a kinetic behaviour is clearly indicative for a reversible O<sub>2</sub>-binding step, hence an equilibrium  $\text{Cu}^{\text{I}}\text{tBu} + \text{O}_2 \rightleftharpoons [\text{CuO}_2]$  is indicated. Below  $-60$  °C, the intercept is close to zero, reflecting an equilibrium that is shifted to the right ( $k_{\text{on}}[\text{O}_2] \gg k_{\text{off}}$ ) with the oxygenated species being predominant in the reaction mixture. However, at temperatures above  $-60$  °C, from the  $y$ -intercept,  $k_{\text{off}}$  can be obtained in addition to  $k_{\text{on}}$ . Reversibility is also confirmed by the experiments described above, demonstrating that O<sub>2</sub> is removed by applying vacuum or gentle warming, and that the

Table 3. Kinetic ( $k_{\text{on}}$ ,  $k_{\text{off}}$ ) and thermodynamic ( $K_{\text{eq}}$ ) parameters for the formation of 1:1 adduct  $[\text{CuO}_2]$  upon low-temperature oxygenation of  $\text{Cu}^{\text{I}}\text{tBu}$  in THF (obtained from cryo-stopped-flow experiments and from the plots in Figure 6).

Activation parameters			
Binding			
$T$ [K]	$k_{\text{on}}$ [ $\text{M}^{-1} \text{s}^{-1}$ ]	$\Delta H_{\text{on}}^{\ddagger}$ [kcal mol $^{-1}$ ]	$\Delta S_{\text{on}}^{\ddagger}$ [cal K $^{-1}$ mol $^{-1}$ ]
233	$2.69 \pm 0.06$	$2.27 \pm 0.18$	$-46.3 \pm 0.8$
223	$2.19 \pm 0.42$		
213	$1.54 \pm 0.18$		
Dissociation			
$T$ [K]	$k_{\text{off}}$ [ $\text{s}^{-1}$ ]	$\Delta H_{\text{off}}^{\ddagger}$ [kcal mol $^{-1}$ ]	$\Delta S_{\text{off}}^{\ddagger}$ [cal K $^{-1}$ mol $^{-1}$ ]
233	$(1.58 \pm 0.02) \times 10^{-2}$	$11.7 \pm 1.9$	$-16.1 \pm 8.2$
223	$(5.6 \pm 1.5) \times 10^{-3}$		
213	$(7.9 \pm 6.5) \times 10^{-4}$		
Thermodynamic parameters			
$T$ [K]	$K_{\text{eq}}^{\text{[a]}}$ [ $\text{M}^{-1}$ ]	$\Delta H^{\circ}$ [kcal mol $^{-1}$ ]	$\Delta S^{\circ}$ [cal K $^{-1}$ mol $^{-1}$ ]
233	$(1.70 \pm 0.04) \times 10^2$	$-10.0 \pm 1.7$	$-32.7 \pm 7.4$
223	$(3.9 \pm 1.3) \times 10^2$		
213	$(2.0 \pm 1.6) \times 10^3$		

[a]  $K_{\text{eq}} = [\text{CuO}_2]/([\text{Cu}^{\text{I}}\text{tBu}][\text{O}_2]) = k_{\text{on}}/k_{\text{off}}$ .

$^{\text{t}}\text{BuP}$  complex is then reconstituted by repeated exposure to  $\text{O}_2$ . In addition, both rate constants of the equilibrium allow determination of the equilibrium constants  $K_{\text{eq}}$  (Table 3).

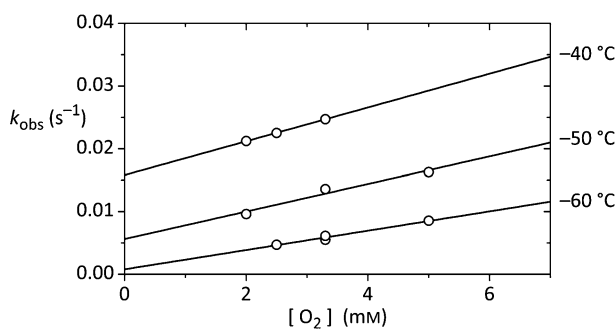


Figure 5. Plots of  $k_{\text{obs}}$  vs. concentration of dioxygen at  $-40$ ,  $-50$  and  $-60$  °C for the activation of dioxygen with  $\text{Cu}^{\text{I}}\text{tBu}$  in THF; data from cryo-stopped-flow measurements.

Activation and equilibrium parameters (Table 3) were determined from Eyring and van't Hoff plots, respectively (Figure 6). The system features a favourable reaction enthalpy of  $\Delta H^{\circ} = (-10.0 \pm 1.7)$  kcal mol $^{-1}$  and an unfavourable reaction entropy of  $\Delta S^{\circ} = (-32.7 \pm 7.4)$  cal K $^{-1}$  mol $^{-1}$ . The thermodynamics determined for 1:1 adduct formation are similar to most copper(I)/dioxygen systems, which have  $\Delta H^{\circ} \approx -7$  to  $-10$  kcal mol $^{-1}$  and  $\Delta S^{\circ} \approx -26$  to  $-33$  cal K $^{-1}$  mol $^{-1}$ .<sup>[2]</sup> In comparison,  $\text{Cu}^{\text{I}}\text{tBu}$  is at the lower edge of those ranges for both parameters. The small enthalpy suggests strong dioxygen binding, which parallels hemocyanin and other biological dioxygen carriers. In contrast, the unfavourable entropy of formation hampers the observation of the copper–oxygen adducts at room temperature in the case of low-molecular-weight systems.<sup>[44]</sup> Therefore, the equilibrium constant for  $\text{Cu}^{\text{I}}\text{tBu}$  is rather small, even at  $-60$  °C ( $2 \times 10^3 \text{ M}^{-1}$ ), whereas noncooperative

oxygen carrier enzymes have significantly larger binding constants at room temperature (e.g., hemocyanin,  $5.7 \times 10^5 \text{ M}^{-1}$ ).<sup>[45]</sup>

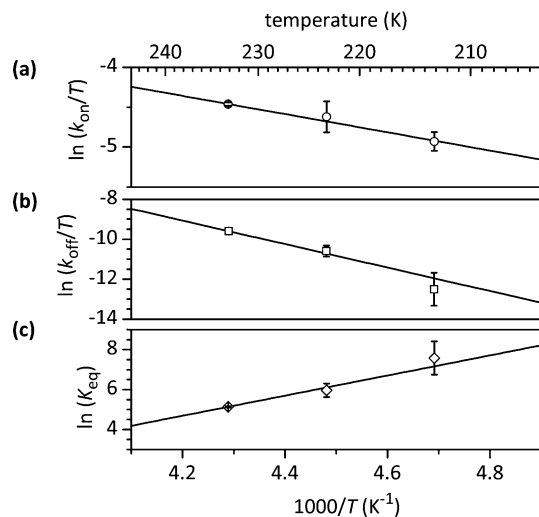


Figure 6. Eyring plots,  $\ln(k T^{-1})$  vs.  $T^{-1}$ , of (a)  $\text{O}_2$  binding ( $k_{\text{on}}$ ) and (b) dissociation ( $k_{\text{off}}$ ) steps with weighted linear regressions. (c) The van't Hoff plot,  $\ln(K_{\text{eq}})$  vs.  $T^{-1}$ , for the equilibrium  $\text{Cu}^{\text{I}}\text{tBu} + \text{O}_2 \rightleftharpoons [\text{CuO}_2]$  ( $K_{\text{eq}} = [\text{CuO}_2]/([\text{Cu}^{\text{I}}\text{tBu}][\text{O}_2]) = k_{\text{on}}/k_{\text{off}}$ ). See Table 3 for derived kinetic and thermodynamic parameters.

Reported activation enthalpies for oxygenation of copper(I) complexes are in a quite narrow range of  $\Delta H_{\text{on}}^{\ddagger} \approx 5$ – $10$  kcal mol $^{-1}$ . Unfavourable activation entropies are generally observed, and are mostly in the range  $\Delta S_{\text{on}}^{\ddagger} \approx -14$  to  $2$  cal K $^{-1}$  mol $^{-1}$ , consistent with an associative mechanism; that is, loss of degrees of freedom upon binding of  $\text{O}_2$ . In comparison to reported systems, for  $\text{Cu}^{\text{I}}\text{tBu}$  an unusually small activation enthalpy of  $\Delta H_{\text{on}}^{\ddagger} = (2.27 \pm 0.18)$  kcal mol $^{-1}$  was found. This suggests that vacant coordination sites are present in  $\text{Cu}^{\text{I}}\text{tBu}$ , and that direct attack of  $\text{O}_2$  can take place without any interference from

solvent (direct oxygenation),<sup>[2,46]</sup> such a very low activation energy is typical of diffusion-controlled processes (1–4 kcal).<sup>[47]</sup> No significant alterations of bonds seem to be necessary to proceed to the transition state. The comparatively small enthalpy might be explained by the fact that Cu<sup>I</sup>*t*Bu is only twofold-coordinated by the BOX ligand, whereas most reported systems, for which kinetic parameters were determined for the 1:1 Cu/O<sub>2</sub> adduct formation, contain tridentate capping ligands.

An associative mechanism is further reflected in the strongly negative activation entropy of  $\Delta S_{\text{on}}^{\ddagger} = (-46.3 \pm 0.8) \text{ cal K}^{-1} \text{ mol}^{-1}$ . Because of this substantial and negative  $\Delta S^{\ddagger}$ , the rate of O<sub>2</sub> binding to Cu<sup>I</sup>*t*Bu in THF at –78 °C ( $k_{\text{obs}} = 0.2 \text{ min}^{-1}$ ) is slow compared with other systems.<sup>[2]</sup> This very unfavourable activation entropy can additionally be blamed for the high thermolability of this system. A reason for this strongly negative entropy might be the bidentate ligand and the vacant coordination side, with respect to coordinative unsaturation of the copper(I) complex: no solvent dissociation is needed to take place upon initial attack of O<sub>2</sub>. The release of coordinated solvent might in fact entropically compensate for the association of O<sub>2</sub> to some extent in the other systems reported previously. However, steric bulk around Cu, arising from the dimethyl groups on the oxazoline rings, might also play a role in the present case (cf. van-der-Waals plots of Cu<sup>I</sup>*t*Bu in Figure S18). The steric demand of the ligand was also suggested to be the reason for particularly unfavourable activation entropies for O<sub>2</sub> binding to other copper complexes,<sup>[44,48]</sup> as well as to Fe<sup>II</sup>{tris(pyridylmethyl)amine}<sup>[49]</sup> and Co<sup>II</sup>(cyclidene)<sup>[47]</sup> systems.

The direct attack of O<sub>2</sub> onto a free coordination site presumably leaves the MeCN bound to Cu in the CuO<sub>2</sub> intermediate adduct, because threefold coordination would be uncommon for Cu<sup>II</sup>. Inspection of the back reaction ( $k_{\text{off}}$  process) also reveals a strongly negative entropy, here  $\Delta S_{\text{off}}^{\ddagger} = (-16.1 \pm 8.2) \text{ cal K}^{-1} \text{ mol}^{-1}$ , indicating that the back reaction also follows an associative mechanism. Here, association of solvent molecules (MeCN or THF) to the CuO<sub>2</sub> complex is likely to be rate-limiting, rather than O<sub>2</sub>-dissociation. A similar kinetic behaviour was observed for, e.g., the formation of a copper(II)–superoxo (1:1) complex.<sup>[50]</sup> Finally, the activation enthalpy  $\Delta H_{\text{off}}^{\ddagger} = (11.7 \pm 1.9) \text{ kcal mol}^{-1}$  reflects a significant reaction barrier for this solvent-association step.

### Isolation and Analysis of Solid Peroxidocopper Compounds

The limited solubility of the <sup>R</sup>P complexes allowed their isolation in good yields in the form of violet to pink powders (Figure S3). Elemental analysis indicates excellent to satisfactory purity for <sup>t</sup>BuP and <sup>H</sup>P and confirms the formulations as  $[\{(\text{R}^{\text{H}}\text{BOX-Me}_2)(\text{THF})\text{Cu}\}_2(\text{O}_2)](\text{PF}_6)_2$ , which includes one coordinated THF molecule per copper ion. For <sup>Me</sup>P, partial decomposition was clear from a slightly greyish colour tint; the analysis showed a comparatively low CHN content, in agreement with loss of coordinated sol-

vent (a partial decomposition is additionally indicated by the methods described below).

Although bidentate ligands suffice in stabilising Cu<sub>2</sub>O<sub>2</sub> species, it should be noted that an additional labile ligand (solvent or counteranion) is generally associated with each metal ion; in case of more common tridentate capping ligands, one of the donors is usually weakly bound.<sup>[1,39]</sup> This parallels the coordination of copper in the role model enzymes (Figure 1). The coordination of THF presumably induces precipitation of the present complexes. However, the differences in coordinating ability towards transition metals between MeCN (coordinating ability index<sup>[51]</sup>  $a^{\text{TM}} = -0.2$ ) and THF (–0.3) are not significant. When in solution, <sup>R</sup>P are stable only at very low temperatures (also reflected by the strongly negative  $\Delta S^{\ddagger}$ ), and – considering the thermolability of Cu/O<sub>2</sub> complexes in general – <sup>t</sup>BuP and <sup>H</sup>P are remarkably insensitive in the solid state. Handling in air at room temperature for short times was straightforward; however, storage for prolonged periods was only possible at low temperatures.

Diffuse reflectance UV/Vis spectroscopy of violet <sup>R</sup>P powder samples shows absorption maxima in accordance with bands observed for the solutions (Figure 7, Table 2). The relative intensities of the absorption bands are obscured due to light scattering by the powders. The spectra exhibit two intense bands at ca. 330 nm and ca. 515 nm, similar to those of the solution spectra. This suggests that the  $\mu\text{-}\eta^2\text{:}\eta^2\text{-peroxodicopper(II)}$  structures are present in both, solution and powder, and it can be presumed that the spectra do not result from a mixture of chromophores. In the case of <sup>Me</sup>P, for which partial decomposition was assumed, the 330 nm feature is also consistent with the solution spectrum and the other solid samples. However, a 493 nm peak is at slightly higher energy and lower intensity, compared with the ca. 515 nm peaks. Furthermore, an additional feature of similar intensity is present at 600 nm; a similar feature is only visible as a shoulder in the case of

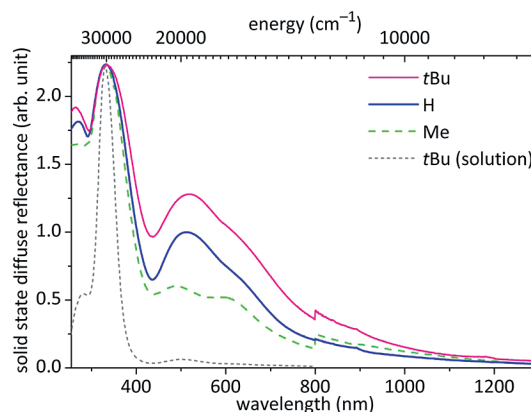


Figure 7. Solid-state UV/Vis/NIR spectra (diffuse reflectance) of <sup>t</sup>BuP and <sup>H</sup>P in KBr powder at room temp. The <sup>Me</sup>P sample reflects some degree of degradation. Spectra are relatively scaled at 330 nm; an artefact is present at the detector/grating change point of 800 nm. For comparison, the spectrum of <sup>t</sup>BuP in THF solution (–78 °C) is depicted (< 800 nm). Spectral properties are compared in Table 2.

<sup>t</sup>BuP and <sup>H</sup>P. For other  $\mu\text{-}\eta^2\text{:}\eta^2\text{-peroxodicopper(II)}$  complexes, where it was possible to isolate a solid sample and to record reflectance spectra, the spectra were also in good agreement with solution data.<sup>[12,18,36]</sup>

RR spectroscopy of the solid samples of <sup>R</sup>P shows the presence of  $\mu\text{-}\eta^2\text{:}\eta^2\text{-coordinated peroxide}$  (Figure 8, Table 2). The respective  $\nu(\text{O-O})$  stretches, increasing with the steric demand of the backbone residue, are detected at 731 (<sup>t</sup>BuP), 735 (<sup>Me</sup>P, Figure S10) and 742  $\text{cm}^{-1}$  (<sup>H</sup>P);  $\nu(\text{Cu-Cu})$  stretches are found at 278 (<sup>t</sup>BuP) and 282  $\text{cm}^{-1}$  (<sup>H</sup>P, <sup>Me</sup>P). The features are essentially unchanged from the solution data for <sup>t</sup>BuP (see above). Isotopic substitution, i.e., oxygenation of the respective copper(I) complex with <sup>18</sup>O<sub>2</sub>, was carried out for <sup>t</sup>BuP and <sup>H</sup>P and effectively shifts the peroxy stretches to 692 and 703  $\text{cm}^{-1}$ , respectively, in both cases with a shift of  $\Delta[\text{O}^{18}\text{O}] = -39 \text{ cm}^{-1}$ , whereas the  $\nu(\text{Cu-Cu})$  features are essentially unchanged, as expected.<sup>[41]</sup> In <sup>H</sup>P, the 742  $\text{cm}^{-1}$  feature is obscured by the PF<sub>6</sub><sup>-</sup> stretch at 745  $\text{cm}^{-1}$ , which, however, is well-separated in the <sup>18</sup>O<sub>2</sub>-labelled sample. The difference spectrum (Figure 8) finally also unveils the  $\nu(\text{O}^{16}\text{O-O}^{16}\text{O})$  stretch. In addition, RR and IR spectroscopy confirm the absence of MeCN and the presence of PF<sub>6</sub><sup>-</sup> counterions in the solid samples (cf. Figures S8–S10), in accordance with elemental analysis.

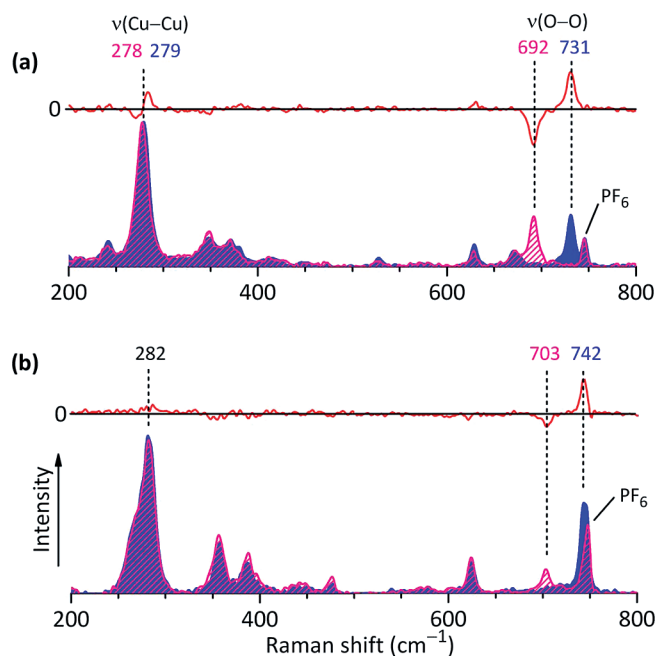


Figure 8. RR spectra of solid powder samples of (a) <sup>t</sup>BuP and (b) <sup>H</sup>P, with <sup>16</sup>O<sup>16</sup>O (blue) and <sup>18</sup>O<sup>18</sup>O (magenta) isotopic composition (632.8 nm laser excitation) and <sup>16</sup>O<sub>2</sub> minus <sup>18</sup>O<sub>2</sub> difference spectra (red). No <sup>16</sup>O/<sup>18</sup>O isotope scrambling was detected.

## Structural Investigations

Synchrotron-based X-ray absorption spectroscopy (XAS) was performed on the <sup>R</sup>P powders. The X-ray absorption near-edge structure (XANES) spectrum established the Cu<sup>II</sup> oxidation states (Figure 9). Low intensity

1s→3d pre-edge transitions at 8979.5 eV were found. Cu<sup>III</sup> in related compounds is characterised by a feature of ca. 2 eV higher energy,<sup>[52,53]</sup> which is not observable in the samples here. The 1s→4p + ligand-to-metal (LMT) shake-down transitions at ca. 8987 eV are only present as weak shoulders with no significant peak intensity; this excludes an oxidation state of Cu<sup>III</sup> that is characterised by a sharp peak on the rising edge.<sup>[52]</sup> Furthermore, Cu<sup>I</sup> is usually indicated by a diagnostic sharp and intense 1s→4p transition at 8984 eV,<sup>[4,54]</sup> with a shape that is dependent on the coordination environment; this feature is also absent in the spectra. Therefore, from the XANES results, a Cu<sup>II</sup> state in all <sup>R</sup>P is concluded, in agreement with side-on  $\mu\text{-}\eta^2\text{:}\eta^2\text{-peroxodicopper(II)}$  complexes. Nonetheless, subtle differences between the samples can be observed in the white-line shape. All samples exhibit a double white-line structure with similar intensity of both white-line components; however, the intensity ratio of the two underlying signals differ. The white-line width of sample <sup>Me</sup>P is reduced compared with those of <sup>H</sup>P and <sup>t</sup>BuP. The white-line signature of <sup>R</sup>P was similarly found for other binuclear  $\mu\text{-}\eta^2\text{:}\eta^2\text{-peroxodicopper}$  complexes.<sup>[4,17,53]</sup>

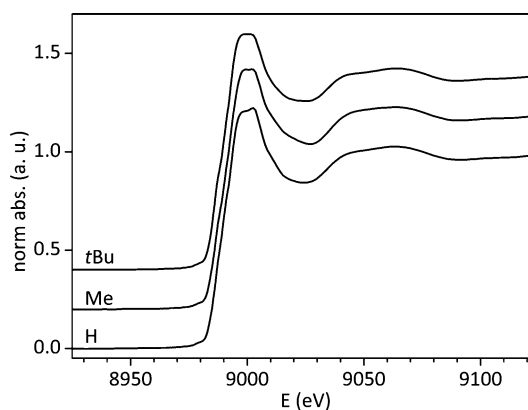


Figure 9. Cu *K*-edge XANES spectra of <sup>t</sup>BuP, <sup>Me</sup>P and <sup>H</sup>P. The spectra are shifted on the ordinate for clarity.

Metric parameters obtained from Cu *K*-edge extended X-ray absorption fine-structure (EXAFS) data (Figure 10, Table 4) are typical for  $\mu\text{-}\eta^2\text{:}\eta^2\text{-peroxodicopper(II)}$  complexes. For comparison, all  $\mu\text{-}\eta^2\text{:}\eta^2\text{-peroxodicopper}$  complexes that have been structurally characterised so far are listed in Table S1.

In <sup>t</sup>BuP and <sup>H</sup>P, the first shell at 1.94 Å agrees well with a fourfold coordination, which is an average value of the two oxygen and two nitrogen atoms from peroxy and BOX ligands [Cu-(N/O)<sub>eq</sub>]. A second light-atom contribution at 2.34 (<sup>t</sup>BuP) or 2.32 Å (<sup>H</sup>P), with a coordination number slightly smaller than one, is attributed to weakly coordinating axial THF (Cu-O<sub>ax</sub>), in accordance with elemental analysis data. These distances are in agreement with each Cu ion having a square-pyramidal geometry. The Cu...Cu distance of (3.51 ± 0.04) Å (<sup>t</sup>BuP) and (3.52 ± 0.04) Å (<sup>H</sup>P) is characteristic for a  $\mu\text{-}\eta^2\text{:}\eta^2\text{-peroxy dicopper(II)}$  complex, which was also confirmed by the Cu...Cu coordination number of one, reflecting the dimeric nature of the complex.

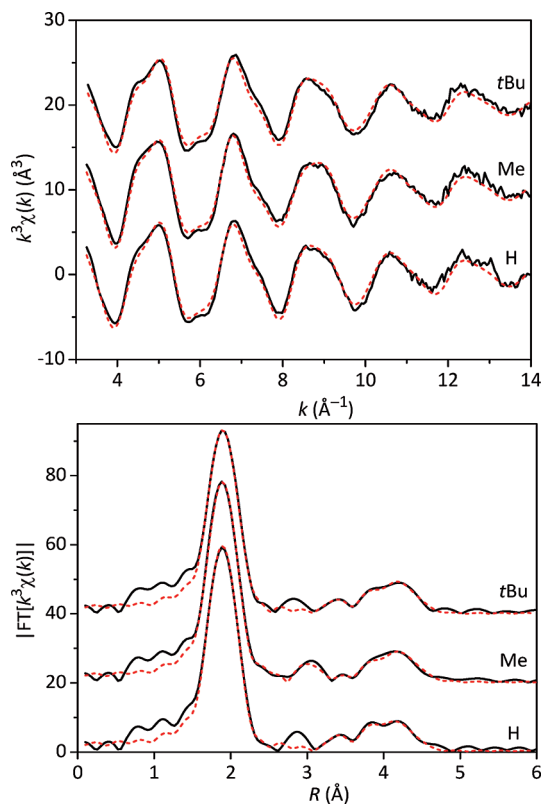


Figure 10. EXAFS spectra  $k^3\chi(k)$  (top) and the corresponding Fourier transformed functions (bottom) of  ${}^t\text{BuP}$ ,  ${}^{\text{Me}}\text{P}$  and  ${}^{\text{H}}\text{P}$ . The experimental spectra are shown as black solid lines, the fitted spectra according to the parameters given in Table 4 are shown as red dashed lines. The spectra are shifted on the ordinate for clarity.

Table 4. Structural parameters obtained by fitting the experimental EXAFS spectra in Figure 10 with theoretical models.

Sample	Abs–Bs <sup>[a]</sup>	$N(\text{Abs})$ <sup>[b]</sup>	$R(\text{Abs–Bs})$ <sup>[c]</sup> [Å]	$\sigma^2$ <sup>[d]</sup> [Å]	$R^{\text{fit}}$ [%] $E_{\text{fit}}$ [eV]
${}^t\text{BuP}$	Cu–(N/O) <sub>eq</sub>	$4.6 \pm 0.5$	$1.94 \pm 0.02$	$0.071 \pm 0.007$	22.48
	Cu–O <sub>ax</sub>	$0.7 \pm 0.1$	$2.34 \pm 0.02$	$0.100 \pm 0.010$	8.2
	Cu $\cdots$ Cu	$1.0 \pm 0.3$	$3.51 \pm 0.04$	$0.095 \pm 0.020$	
	Cu–O–Cu <sub>MS</sub>	$3.5 \pm 0.7$	$3.72 \pm 0.04$	$0.102 \pm 0.020$	
	Cu–NC <sub>MS</sub>	$9.0 \pm 1.8$	$4.28 \pm 0.04$	$0.102 \pm 0.020$	
${}^{\text{H}}\text{P}$	Cu–(N/O) <sub>eq</sub>	$4.8 \pm 0.5$	$1.94 \pm 0.02$	$0.071 \pm 0.007$	19.71
	Cu–O <sub>ax</sub>	$0.5 \pm 0.1$	$2.32 \pm 0.02$	$0.100 \pm 0.010$	7.4
	Cu $\cdots$ Cu	$0.9 \pm 0.3$	$3.52 \pm 0.04$	$0.087 \pm 0.020$	
	Cu–O–Cu <sub>MS</sub>	$3.9 \pm 0.7$	$3.73 \pm 0.04$	$0.102 \pm 0.020$	
	Cu–NC <sub>MS</sub>	$7.8 \pm 1.6$	$4.29 \pm 0.04$	$0.100 \pm 0.020$	
${}^{\text{Me}}\text{P}$	Cu–(N/O)	$5.4 \pm 0.5$	$1.94 \pm 0.02$	$0.074 \pm 0.007$	20.33
	Cu $\cdots$ Cu	$0.6 \pm 0.1$	$2.93 \pm 0.03$	$0.100 \pm 0.010$	7.9
	Cu–Cu	$0.2 \pm 0.1$	$3.49 \pm 0.04$	$0.032 \pm 0.010$	
	Cu–O–Cu <sub>MS</sub>	$1.6 \pm 0.7$	$3.79 \pm 0.04$	$0.084 \pm 0.017$	
	Cu–NC <sub>MS</sub>	$9.9 \pm 2.0$	$4.29 \pm 0.04$	$0.107 \pm 0.022$	

[a] Abs = X-ray absorbing atom, Bs = backscattering atom. [b] Number of neighbour backscattering atoms. [c] Distance between Abs and Bs. [d] Debye–Waller-like factor. [e] Quality of fit. [f] Shift between experimental and theoretical EXAFS function.

Surprisingly, Cu–C shells around 3 Å could not be adjusted with statistical significance, which indicates a rather high degree of disorder in the solid samples. Higher shells at distances larger than 3.5 Å are caused by Cu–O–Cu and Cu–N–C multiscattering (MS) paths, that are similarly de-

scribed.<sup>[17,54]</sup> The Cu $\cdots$ Cu distance and the corresponding Cu–O–Cu multiscattering path (3.72 Å) are in agreement with the Cu<sub>2</sub>O<sub>2</sub> core having a slightly butterfly-shaped geometry, which is confirmed by DFT calculations for  ${}^t\text{BuP}$  (see below). In contrast to these  $\mu\text{-}\eta^2\text{:}\eta^2\text{-peroxodicopper(II)}$  complexes, end-on 1,2-*trans*-peroxodicopper(II) complexes would show a Cu $\cdots$ Cu distance of ca. 4.6 Å, whereas bis( $\mu$ -oxo)dicopper(III) complexes are characterised by a short Cu $\cdots$ Cu separation of ca. 2.80 Å.<sup>[1]</sup> Furthermore, the thermal degradation products of  ${}^t\text{BuP}$ , bis(hydroxo)dicopper(II) complexes, have Cu $\cdots$ Cu distances of 3.0 Å as determined by X-ray crystallography (see below). None of those Cu $\cdots$ Cu distances could be detected in  ${}^{\text{H}}\text{P}$  and  ${}^t\text{BuP}$ .

In contrast to  ${}^t\text{BuP}$  and  ${}^{\text{H}}\text{P}$ , no second light-atom contribution could be adjusted for  ${}^{\text{Me}}\text{P}$  in a statistically significant manner. Instead, the first contribution exhibits a slightly higher coordination number than in  ${}^t\text{BuP}$  and  ${}^{\text{H}}\text{P}$ , suggesting that a solvent contribution cannot be resolved anymore, but is averaged with the ligand contribution. In  ${}^{\text{Me}}\text{P}$ , two Cu $\cdots$ Cu shells were necessary to achieve a satisfactory quality of fit. The shorter one found at 2.93 Å can be interpreted by the presence of a bis( $\mu$ -hydroxo)dicopper(II) species, whereas the longer one (3.49 Å) is still in agreement with the peroxo species found in the case of  ${}^t\text{BuP}$  and  ${}^{\text{H}}\text{P}$ . The coordination numbers of 0.6 and 0.2 suggest that the peroxo species represents the minor fraction. It should also be noted that the Cu $\cdots$ Cu coordination numbers do not add to unity, therefore a small fraction of monomeric species could be also present. The reduced fraction of peroxo species is also reflected in the reduced Cu–O–Cu multiple scattering contribution. However, the remaining presence of Cu–NC multiple scattering indicates that the ligand scaffold is still intact in the present species.

## Theoretical Investigations

Density functional theory (DFT) was applied to model the structure of  ${}^t\text{BuP}$ , with MeCN as coordinating solvent. A DFT spin-unrestricted formalism has been applied to first calculate a high-spin triplet state ( $S = 1$ ) geometry, which was then used to calculate the spin-polarized broken-symmetry (BS) solution.<sup>[55,56]</sup> The spin on one copper atom was flipped in expectation of an antiferromagnetically coupled ( $M_S = 0$ ) state. In the successfully obtained BS solution, Mulliken spin populations at the copper atoms are +0.4930 and –0.4932. Figure 11 shows the obtained geometry and a plot of the spin-density.

UHF natural orbitals are depicted in Figure S14. The computations reproduce well the experimental bond lengths from EXAFS data within a mean error of ca. 2% (Table S2) as well as the suggested slight butterfly-shape of the Cu<sub>2</sub>O<sub>2</sub> core (Cu–O–O–Cu torsion angle is 152°); the nature of the HOMO of the butterfly structure is reminiscent of that previously reported for such structure.<sup>[57]</sup> The computed Cu $\cdots$ Cu separation of 3.56 Å is only slightly overestimated compared with the experimental distance of 3.51 Å derived from EXAFS data.

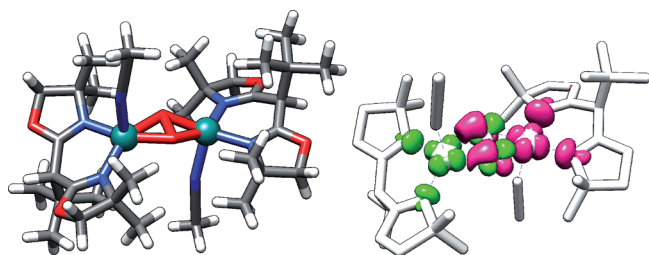


Figure 11. Broken symmetry ( $M_S = 0$ ) DFT geometry-optimised coordinates of  $t\text{BuP}$  (left) and spin-density plot (right, isovalue = 0.004). Colour code: Cu, teal; N, blue; O, red; C, grey; H, white. B3LYP/def2-TZVPP (Cu,N,O)/def2-SVP(C,H) level of theory.

Using time-dependent (TD) DFT, the electronic spectrum of  $t\text{BuP}$  was successfully reproduced (Figure 12, see the Supporting Information for details). The calculated spectrum closely corresponds with the experimental spectrum. The intensity pattern for the UV/Vis absorptions agrees with the experimental spectrum and with the typical pattern<sup>[1]</sup> for a  $\mu\text{-}\eta^2\text{:}\eta^2\text{-peroxodicopper(II)}$  complex [higher energy  $\pi_{\sigma^*}(\text{O}_2^{2-}) \rightarrow \text{Cu}^{\text{II}}$  more intense than lower energy  $\pi_{\nu^*}(\text{O}_2^{2-}) \rightarrow \text{Cu}^{\text{II}}$  transition; intensities ca. 25:1].

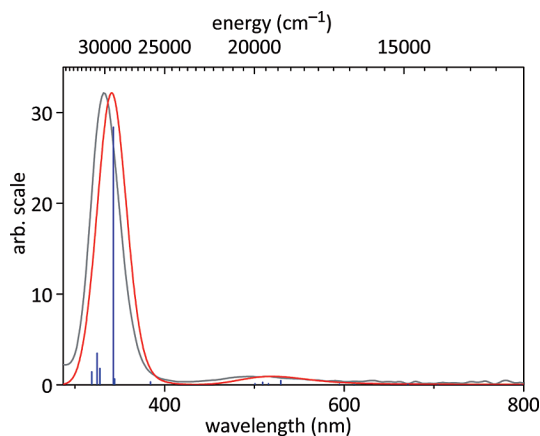


Figure 12. UV/Vis absorption spectra of  $t\text{BuP}$ . Grey line: experimental low-temperature UV/Vis spectrum ( $\lambda_{\text{max}} = 333, 500 \text{ nm}$ ; THF,  $-78 \text{ }^\circ\text{C}$ ). Blue sticks: computed TD-DFT transitions. Red line: convolution of calculated transitions (full width at half maximum:  $3000 \text{ cm}^{-1}$ ), which reproduces well the experimental solution spectrum ( $\lambda_{\text{max}} = 340, 520 \text{ nm}$ ); the intensities are scaled relatively.

## Magnetic Coupling

Examples of experimentally determined magnetic exchange coupling constants for copper–dioxygen systems are scarce,<sup>[36,40,58–60]</sup> due to the thermal lability of most complexes. Usually, EPR silence is taken as an indication of a diamagnetic ground state, and “normal” NMR spectroscopic behaviour (i.e., no paramagnetically shifted resonances) is taken as evidence for the presence of strong antiferromagnetic coupling. Magnetic susceptibility measurements using a SQUID magnetometer confirm the  $S = 0$  ground state of solid  $t\text{BuP}$  and  $\text{HP}$ , resulting from very strong antiferromagnetic coupling between the cupric ions. Simulations of the data show that the lower limits of exchange

coupling are both extremely high,  $-2J \geq 1000 \text{ cm}^{-1}$  for  $t\text{BuP}$  and  $-2J \geq 1200 \text{ cm}^{-1}$  for  $\text{HP}$ , based on  $H = -2J \cdot S_1 \cdot S_2$  (Figure 13). Above room temp., up to  $330 \text{ K}$ , a slight increase of  $\chi_{\text{mol}}T$  is discernible in the case of solid  $\text{HP}$  (grey circles, not considered in the fits). A subsequent measurement after cooling to  $295 \text{ K}$  showed increased  $\chi_{\text{mol}}T$  compared with the initial values for the pristine sample around this temperature (grey square), suggesting that irreversible decomposition of the complex occurred above room temp.

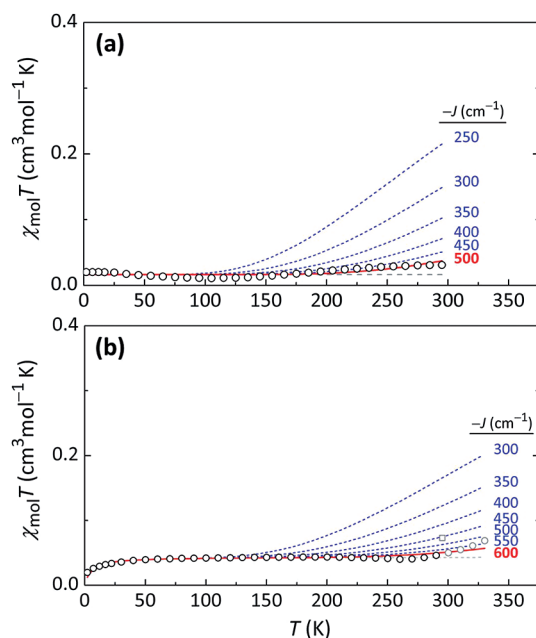


Figure 13. Plots of  $\chi_{\text{mol}}T$  vs.  $T$  (circles) for (a)  $t\text{BuP}$  and (b)  $\text{HP}$  obtained from SQUID measurements at  $0.5 \text{ T}$ . The red solid lines each correspond to the best fit for two antiferromagnetically coupled  $S = 1/2$  ions with  $g = 2.0$ . Additional fit parameters: temperature-independent paramagnetism [ $TIP$  of (a)  $990 \times 10^{-6}$  and (b)  $185 \times 10^{-6} \text{ cm}^3 \text{ mol}^{-1} \text{ K}$ ] and paramagnetic impurity [grey dashed lines,  $PI$  of (a)  $4$  and (b)  $11.6 \text{ mol}\%$  for magnetic uncoupled  $\text{Cu}^{\text{II}}$  species as likely impurities]. The fits give lower limits of the exchange coupling constant  $-J$  of (a)  $\geq 500 \text{ cm}^{-1}$  and (b)  $\geq 600 \text{ cm}^{-1}$ . The blue lines represent simulations assuming weaker coupling (smaller  $-J$  values). In (b), a change in the sample occurred  $> 290 \text{ K}$  (grey circles), indicated by a subsequent measurement at  $295 \text{ K}$  (grey square); due to this, the grey data points were not considered in the fits.

An equally large singlet–triplet splitting of  $-2J \geq 600 \text{ cm}^{-1}$  was found for oxyhemocyanine.<sup>[58]</sup> Coupling constants could also be determined for synthetic model systems in a few cases. Similar values were found for two  $\mu\text{-}\eta^2\text{:}\eta^2\text{-peroxo}$  bridged model systems,  $-2J \geq 600$ <sup>[59]</sup> and  $-2J \geq 800 \text{ cm}^{-1}$ ,<sup>[36]</sup> as well as for a model compound with *trans*-1,2-peroxo-coordination ( $-2J \geq 600 \text{ cm}^{-1}$ ).<sup>[59,60]</sup> Only recently was a weakly coupled peroxo-dicopper(II) complex reported ( $-2J = 144 \text{ cm}^{-1}$ ), characterised by a *cis*-1,2-peroxo binding mode and an acute  $\text{Cu-O-O-Cu}$  torsion of  $65^\circ$ .<sup>[40]</sup> Our DFT calculations for  $t\text{BuP}$  are in agreement with the experimentally determined coupling ( $-2J \approx 3000 \text{ cm}^{-1}$ ; see the Supporting Information for details), and are furthermore in the range of calculations for other  $\mu\text{-}\eta^2\text{:}\eta^2\text{-peroxo}$ -dicopper(II) systems.<sup>[61]</sup>

### Thermal Degradation

After warming to room temp., solutions of intense violet  $t^{\text{Bu}}\text{P}$  bleach or turn bluish; the violet powder of  $t^{\text{Bu}}\text{P}$  also turns light-blue after some time at room temp., which is indicative of the formation of the corresponding bis-(hydroxo)-bridged  $\text{Cu}_2(\text{OH})_2$  complex as the decomposition product. The decomposition was also clearly evident in the Raman spectrum of this powder, which lacks the intense archetypical  $\nu(\text{O}-\text{O})$  and  $\nu(\text{Cu}-\text{Cu})$  features of  $t^{\text{Bu}}\text{P}$  (Figure S11). The  $[(t^{\text{Bu,H}}\text{BOX-Me}_2)_2\text{Cu}_2(\text{OH})_2(\text{PF}_6)]^+$  ion was identified in the high-resolution ESI mass spectrum (Figure S12). A solution of  $^{18}\text{O}$ -labelled  $t^{\text{Bu}}\text{P}$  at room temp. afforded the corresponding  $^{18}\text{O}$ -labelled bis(hydroxo) complex. However, approximately 50%  $^{16}\text{O}/^{18}\text{O}$  isotope scrambling was evident, and it is expected that an exchange with water from solvents or air is relatively fast. Similarly, the IR spectrum of a powder sample, prepared by leaving  $^{18}\text{O}$ -labelled  $t^{\text{Bu}}\text{P}$  at room temp. and in air for some days, showed no difference in OH stretch compared to a sample with normal isotopic composition.

Single crystals of  $[(t^{\text{Bu,H}}\text{BOX-Me}_2)(\text{L})\text{Cu}(\text{OH})]_2(\text{PF}_6)_2$  could be isolated from two different solutions and were analysed by X-ray diffraction (L is either THF/MeCN or  $\text{H}_2\text{O}$ ; Figure 14). Metric parameters of the central  $\text{Cu}^{\text{II}}_2(\text{OH})_2$  units (Table 5), such as the  $\text{Cu}\cdots\text{Cu}$  separation, are similar to those reported for other  $\text{Cu}^{\text{II}}_2(\text{OH})_2$  dimers.<sup>[62]</sup> The complex resides on a crystallographically imposed inversion centre; the bulky  $t^{\text{Bu}}$  ligand residues are located on opposite sides of the  $\text{Cu}_2(\text{OH})_2$  core. All copper(II) ions are found in square-pyramidal environment ( $\tau = 0.02$  and  $0.10$ , respectively).<sup>[63]</sup> In analogy to  $t^{\text{Bu}}\text{P}$ , solvent ligands are weakly bound ( $2.2\text{--}2.3 \text{ \AA}$ ) in the axial positions. We found no indication for any oxidative degradation of the  $t^{\text{Bu,H}}\text{BOX-Me}_2$  ligand itself. This is important, consider-

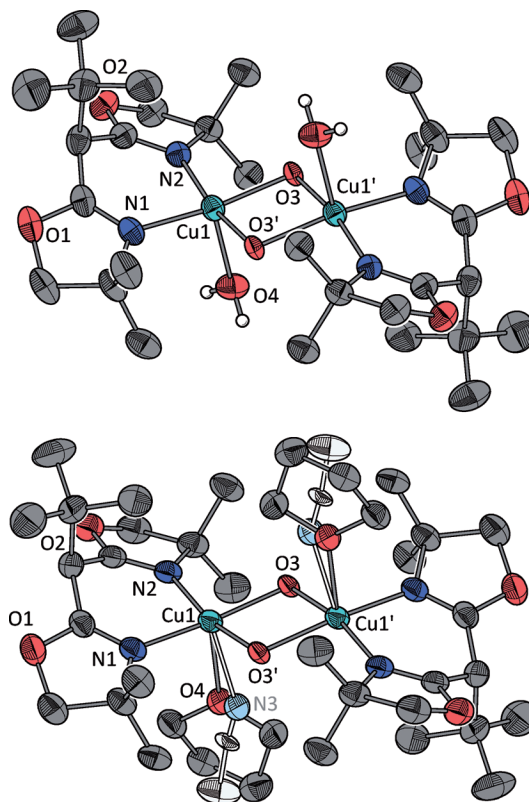


Figure 14. X-ray solid-state molecular structures of  $[(\text{H}_2\text{O})-(t^{\text{Bu,H}}\text{BOX-Me}_2)\text{Cu}(\text{OH})_2](\text{PF}_6)_2$  (top) and  $[(\text{THF})_{0.85}(\text{MeCN})_{0.15}-(t^{\text{Bu,H}}\text{BOX-Me}_2)\text{Cu}(\text{OH})_2](\text{PF}_6)_2$  (bottom). ORTEP plots with significant atoms labelled. Displacement ellipsoids are drawn at the 50% probability level; anions and most hydrogen atoms have been omitted for clarity; MeCN located at a second site due to crystallographic disorder are drawn in lighter shade; symmetry transformations used to generate equivalent atoms (') in each complex:  $1 - x, 1 - y, -z$ . See Figure S19 for further representations. Significant interatomic distances and angles are listed in Table 5.

Table 5. Selected atom distances and bond angles for  $[(\text{L})(t^{\text{Bu,H}}\text{BOX-Me}_2)\text{Cu}(\text{OH})]_2(\text{PF}_6)_2$  with L = THF/MeCN or  $\text{H}_2\text{O}$ , shown in Figure 14.

Atoms 1,2 L	$d$ 1,2 [ $\text{\AA}$ ]		Atoms 1,2,3 L	Angle 1,2,3 [ $^\circ$ ]	
	THF/MeCN	$\text{H}_2\text{O}$		THF/MeCN	$\text{H}_2\text{O}$
$\text{Cu1}\cdots\text{Cu1}'$	3.0435(6)	2.9968(7)	$\text{N1}-\text{Cu1}-\text{N2}$	91.65(10)	91.82(10)
$\text{O3}\cdots\text{O3}'$	2.406(2)	2.450(3)	$\text{O3}-\text{Cu1}-\text{O3}'$	76.65(7)	78.54(8)
$\text{Cu1}-\text{N1}$	1.979(2)	1.981(3)	$\text{N1}-\text{Cu1}-\text{O3}'$	94.54(9)	93.75(9)
$\text{Cu1}-\text{N2}$	1.986(2)	1.986(2)	$\text{N2}-\text{Cu1}-\text{O3}$	95.16(8)	93.85(9)
$\text{Cu1}-\text{O3}$	1.9376(16)	1.9348(17)	$\text{N1}-\text{Cu1}-\text{O3}$	166.15(9)	163.65(9)
$\text{Cu1}-\text{O3}'$	1.9420(17)	1.9361(17)	$\text{N2}-\text{Cu1}-\text{O3}'$	167.64(8)	169.71(9)
$\text{Cu1}-\text{O4}$	2.288(4)	2.246(2)	$\text{N1}-\text{Cu1}-\text{O4}$	94.40(12)	100.08(10)
$\text{Cu1}-\text{N3}$	2.35(4)		$\text{N2}-\text{Cu1}-\text{O4}$	92.35(10)	95.87(9)
			$\text{O3}-\text{Cu1}-\text{O4}$	97.35(10)	94.58(9)
			$\text{O3}'-\text{Cu1}-\text{O4}$	97.83(9)	91.67(9)
			$\text{N1}-\text{Cu1}-\text{N3}$	99.7(8)	
			$\text{N2}-\text{Cu1}-\text{N3}$	101.5(7)	
			$\text{O3}-\text{Cu1}-\text{N3}$	90.8(8)	
			$\text{O3}'-\text{Cu1}-\text{N3}$	88.1(7)	
			$\text{O4}-\text{Cu1}-\text{N3}^{\text{[a]}}$	10.7(6)	
			$\text{Cu1}-\text{O3}-\text{Cu1}'$	103.35(7)	101.46(8)
			$\phi(\text{Cu1}-\text{O3}-\text{O3}'-\text{Cu1}')$	180	180
			$\tau$ value <sup>[b]</sup>	0.02	0.10

[a] Note that this angle is between two disordered molecules. [b]  $\tau = (\beta - \alpha)/60^\circ$ ; <sup>[63]</sup> trigonal bipyramidal,  $\tau = 1$ ; square pyramidal,  $\tau = 0$ .

ing that intramolecular ligand oxygenation or oxidation has often been observed in  $\text{Cu}_2\text{O}_2$  complexes with other capping ligands.<sup>[2,64]</sup>

No analogous  $\text{Cu}_2(\text{OH})_2$  complex has been isolated from  $^{\text{H}}\text{P}$  so far. Experimental evidence suggests, however, that the ligand is oxygenated at the backbone upon degradation of  $^{\text{H}}\text{P}$ . When dissolved in  $\text{CH}_2\text{Cl}_2$  or acetone at room temp., solutions of  $^{\text{H}}\text{P}$  turn red to brown. Analysis by ESI mass spectrometry indicated the presence of oxygenated ligand. The observed base peak ( $m/z$  225.1, [ $^{\text{O}}\text{BOX-Me}_2 + \text{H}$ ] $^+$ ) matches the pattern expected for the oxygenated ligand with bridging C=O as the backbone. It was so far possible to isolate only a small amount of oxygenated ligand  $^{\text{O}}\text{BOX-Me}_2$ . Analysis by  $^1\text{H}$  and  $^{13}\text{C}$  NMR spectroscopy proved the absence of any H atoms at the C atom linking the two oxazoline rings, and also a corresponding cross-peak signal was absent in an  $^1\text{H}, ^{13}\text{C}$ -HSQC experiment. Such ligand oxygenation reactivity is likely, when considering the closely related diketiminate (NacNac) ligand class. It has previously been shown that a NacNac ligand is oxygenated in an analogous fashion by heating to 50 °C in air for 12 h with  $\text{Cu}(\text{OAc})_2$ .<sup>[65]</sup> Further investigations are ongoing to unravel mechanistic details of the ligand oxygenation upon thermal degradation of  $^{\text{H}}\text{P}$ .

### Reactivity Towards External Substrates

$^{\text{tBu}}\text{P}$  was used for preliminary reactivity studies because the stability and solubility of  $^{\text{Me}}\text{P}$  and  $^{\text{H}}\text{P}$  are limited. The results showed that  $^{\text{tBu}}\text{P}$  reacts with 2,4-di-*tert*-butylphenol to give the C–C coupling product 3,3',5,5'-tetra-*tert*-butyl-2,2'-biphenol, whereas *ortho*-hydroxylation was not observed. Although there may be electronic reasons associated with the butterfly-type core,<sup>[57]</sup> it should be noted that  $^{\text{tBu}}\text{P}$  is quite compact due to the bulky dimethyl and *tert*-butyl substituents, as well as the bound solvent molecules [cf. van der Waals plots of the bis(hydroxo)dicopper(II) complex in Figure S19]. Thus, the central  $\text{Cu}_2\text{O}_2$  core seems to be difficult to access for large substrates. Further reactivity studies are ongoing.

### Conclusions

$\text{Cu}^{\text{tBu}}$  was shown to reversibly bind dioxygen and to serve as a new functional hemocyanin model. The resulting  $\mu\text{-}\eta^2\text{:}\eta^2\text{-peroxo}$ dicopper(II) complex  $^{\text{tBu}}\text{P}$  has been characterised by a variety of methods, both in solution and in the solid state, and thermodynamic and kinetic parameters relating to its formation have been determined. Studies on the two analogous  $\mu\text{-}\eta^2\text{:}\eta^2\text{-peroxo}$ dicopper(II) complexes  $^{\text{H}}\text{P}$  and  $^{\text{Me}}\text{P}$  support the results, but these compounds exhibit more pronounced thermal lability and limited solubility, which is inherent to this class. This work demonstrates that simple bis(oxazoline) derivatives, which represent a privileged ligand class, are suitable scaffolds for supporting biomimetic  $\text{Cu}/\text{O}_2$  species. A rich and versatile  $\text{Cu}/\text{O}_2$  chemis-

try can be expected because numerous BOX derivatives are readily available.

### Experimental Section

**Materials and Instrumentation:** Unless otherwise stated, all solvents used were of commercially available analytical, spectroscopic or HPLC grade. Diethyl ether was dried by heating to reflux with sodium/benzophenone, tetrahydrofuran (THF) with potassium/benzophenone and both were distilled under an argon atmosphere. Methylene chloride ( $\text{CH}_2\text{Cl}_2$ ) was degassed and then dried by a series of drying columns in an MBraun solvent purification system (MB-SPS 800). Acetone was degassed and dried by stirring over boron trioxide ( $\text{B}_2\text{O}_3$ ) for 24 h with a desiccant loading of 5% w/v and then distilled under argon.<sup>[66]</sup> All solvents were kept in storage flasks with an attached J. Young PTFE valve under an atmosphere of dry argon. Argon 5.0 (99.999%) was passed through a column of SICAPENT (phosphorus pentoxide on inert carrier). Preparation and handling of air-sensitive compounds were performed under an argon atmosphere using standard Schlenk techniques or in an MBraun LABmaster SP inert atmosphere glovebox workstation, filled with nitrogen with glovebox atmosphere levels of oxygen and moisture < 0.1 ppm. Deoxygenation of solvents and solutions was effected by either sparging with argon for 15–20 min or repeated freeze–pump–thaw cycles. All chemicals were purchased from common distributors and were used without further purification. Dioxygen 4.5 (99.995%) was from Linde; isotopically enriched dioxygen-18 ( $^{18}\text{O}_2$ ) was from Campro Scientific and was of 99.7% purity with the isotopic composition  $^{18}\text{O}/^{17}\text{O}/^{16}\text{O}$  of 97.1:0.9:2.0 atom-%. Tetrakis(acetonitrile)copper(I) hexafluorophosphate,  $[\text{Cu}(\text{MeCN})_4](\text{PF}_6)_6$ , was synthesised by following a reported method.<sup>[67]</sup> The ligands  $^{\text{R,H}}\text{BOX-Me}_2$  (R = H, Me, *t*Bu) were prepared by following the procedures we reported recently.<sup>[35]</sup>

NMR spectra were recorded at room temperature (unless otherwise noted) with a Bruker Avance DRX 500 MHz, Avance 300 MHz or 400 MHz spectrometer.  $^1\text{H}$  and  $^{13}\text{C}$  chemical shifts ( $\delta$ ) are reported in ppm relative to  $\text{SiMe}_4$  and were determined relative to the residual solvent peaks.  $^{15}\text{N}$ ,  $^{31}\text{P}$  and  $^{19}\text{F}$  chemical shifts are reported in ppm relative to nitromethane, phosphoric acid and trichlorofluoromethane respectively, and were referenced externally using the solvents deuterium lock frequency. Multiplicities are indicated [br (broadened), s (singlet), d (doublet), sept (septet)].  $^{15}\text{N}$  NMR resonances were recorded by using  $^1\text{H}, ^{15}\text{N}$ -HMBC experiments. Assignment of all  $^1\text{H}$  and  $^{13}\text{C}$  NMR resonances was possible, using  $^1\text{H}, ^{13}\text{C}$ -HSQC and  $^1\text{H}, ^{13}\text{C}$ -HMBC experiments when necessary. Electrospray mass spectra (ESI-MS) were recorded with an Applied Biosystems API 2000 spectrometer or a Bruker HCTultra (high-capacity ion trap) spectrometer with an additional inlet connected to an MBraun glovebox, and capable of further fragmentation of ions ( $\text{MS}^2$ ). ESI $^{+/-}$  indicates that the detector was used either in positive or negative mode. High-resolution mass spectra (HRMS) were recorded with a Bruker APEX IV spectrometer (Fourier Transform Ion Cyclotron Resonance, FTICR-ESI-MS) or a Bruker micrOTOF (time of flight, TOF-ESI-MS) spectrometer. High-resolution ions and isotopic patterns were simulated with Bruker Compass DataAnalysis 4.0. Vibrational (IR) spectra were recorded with a Digilab Excalibur Series FTS 3000. Samples were ground with potassium bromide and pressed to a pellet. Peaks are reported with the following intensities: s (strong), m (medium), w (weak) and br (broad);  $\nu_{\text{as}}$  and  $\nu_{\text{s}}$  indicate asymmetric and symmetric stretching modes respectively. Resonance Raman (RR) spectra were measured with a Horiba LabRAM HR 800 Raman spectrometer equipped

with an open-electrode CCD detector using a backscattering microscope optic. A He/Ne mixed-gas laser was used for excitation; spectra were recorded with an excitation wavelength  $\lambda_{\text{ex}} = 632.8$  nm. Thermally unstable samples were measured in a CryoVac Konti-Cryostat-Mikro at 213 K, cooled by the flow of liquid N<sub>2</sub>-cooled N<sub>2</sub> gas. Solutions of <sup>R</sup>P were generated directly in the measuring cell by oxygenation with O<sub>2</sub> gas. Solid samples were measured in air at ambient temperature. Isotopic substitution was achieved by oxygenating with <sup>18</sup>O<sub>2</sub> gas. The recorded spectra were processed with Horiba LabSpec 5 software. The compositions of C, H and N were determined with an Elementar 4.1 vario EL 3 elemental analyser and were carried out by the Analytical Laboratory of the Institute of Inorganic Chemistry at the University of Göttingen. UV/Vis/NIR electronic spectra were recorded at room temperature with a Varian Cary 50 Bio spectrophotometer. Low-temperature measurements were performed directly in the reaction solution with an all-quartz immersion probe in a custom-made reaction tube (transmission measurement with 1 mm optical path, Hellma Analytics). The spectra were recorded by the use of a fibre-optical connection and analysed by Cary Win UV and OriginLab OriginPro 8.5.1 software. The temperature was maintained with a dry ice in acetone cooling bath (−78 °C) or a dry ice in ethylene glycol cooling bath (ca. −20 °C). Oxygenation of the copper(I) complex was achieved by introduction of molecular dioxygen into cooled reaction solutions by bubbling through a stainless steel syringe needle, or by slow injection of complex solution into an oxygen saturated and cooled solution. Subsequent removal of excess dioxygen was carried out by bubbling with argon and/or repeated vacuum–argon cycles. Extinction coefficients ( $\epsilon$ ) are uncorrected for solvent contraction (THF ca. 10%, from ambient temperature to 195 K). Powder samples were measured with a Varian Cary 5000 instrument by using a Harrick Praying Mantis diffuse reflection accessory. Samples were ground with potassium bromide and measured in a microsampling cup at room temperature; *sh* stands for an absorption shoulder.

**[<sup>t</sup>Bu,<sup>H</sup>BOX-Me<sub>2</sub>)Cu(MeCN)]PF<sub>6</sub> (Cu<sup>t</sup>Bu). Method 1:** <sup>t</sup>Bu,<sup>H</sup>BOX-Me<sub>2</sub> (50 mg, 188  $\mu$ mol, 1.05 equiv.) was dissolved in anhydrous CH<sub>2</sub>Cl<sub>2</sub> (40 mL) under an atmosphere of argon. The solution was sparged for ca. 15 min with argon to ensure the absence of oxygen. [Cu(MeCN)<sub>4</sub>]PF<sub>6</sub> (66 mg, 170  $\mu$ mol, 1.00 equiv.) was added and the mixture was stirred for 30 min until all salt was dissolved. A colourless solution was obtained. The solvent was removed in vacuo and the resulting residue was heated to 80 °C under vacuum to remove excess ligand to obtain Cu<sup>t</sup>BOX quantitatively as an air-sensitive white powder.

**Method 2:** <sup>t</sup>Bu,<sup>H</sup>BOX-Me<sub>2</sub> (24 mg, 90  $\mu$ mol) was dissolved in anhydrous THF (5 mL) under an atmosphere of argon in a small Schlenk flask. The solution was sparged for ca. 15 min with argon to ensure the absence of oxygen. [Cu(MeCN)<sub>4</sub>]PF<sub>6</sub> (34 mg, 90  $\mu$ mol, 1.0 equiv.) was added and the obtained colourless solution was stirred for some minutes. The flask was then linked to a second Schlenk flask, containing anhydrous, degassed diethyl ether (40 mL), by a bent glass adapter. The slow gaseous diffusion of Et<sub>2</sub>O into the THF solution afforded small crystalline white rods of the copper(I) complex after a few days. The single crystals obtained were of high quality and were suitable for X-ray structure determination. The supernatant was removed and the residue was thoroughly washed with anhydrous degassed Et<sub>2</sub>O (5  $\times$  4 mL) under argon by using a syringe with a stainless steel needle. After drying in vacuo, Cu<sup>t</sup>Bu (12 mg, 26%) was obtained as a white crystalline solid. MS (ESI<sup>+</sup>, MeCN): *m/z* (%) = 595.3 (17) [2 BOX + Cu]<sup>+</sup>, 370.0 (100) [(BOX)Cu(MeCN)]<sup>+</sup>, 329.0 (32) [(BOX)-Cu]<sup>+</sup>. <sup>1</sup>H NMR (400 MHz, CD<sub>2</sub>Cl<sub>2</sub>):  $\delta$  = 4.25 (d, *J* = 8.9 Hz, 2 H,

2CHH), 4.21 (d, *J* = 8.9 Hz, 2 H, 2CHH), 3.29 (s, 1 H, CH), 2.28 (s, 3 H, MeCN), 1.39 (s, 6 H, 2CH<sub>3</sub>), 1.38 (s, 6 H, 2CH<sub>3</sub>), 1.10 (s, 9 H, <sup>t</sup>Bu) ppm. <sup>13</sup>C{<sup>1</sup>H} NMR (101 MHz, CD<sub>2</sub>Cl<sub>2</sub>):  $\delta$  = 168.0 (C=N), 80.3 (CH<sub>2</sub>), 68.1 (CMe<sub>2</sub>), 48.5 (CH), 37.0 (CMe<sub>3</sub>), 28.8 (2Me), 28.7 (CMe<sub>3</sub>), 28.6 (2Me), 3.2 (MeCN) ppm, MeCN was not observed. <sup>15</sup>N NMR (30 MHz, CD<sub>2</sub>Cl<sub>2</sub>):  $\delta$  = −161.4 (C=N) ppm, MeCN was not observed. UV/Vis (THF or acetone): no absorption (300–800 nm).

**[<sup>H,H</sup>BOX-Me<sub>2</sub>)Cu(MeCN)]PF<sub>6</sub> (Cu<sup>H</sup>H):** <sup>H,H</sup>BOX-Me<sub>2</sub> (63 mg, 0.30 mmol) was dissolved in anhydrous THF (40 mL) under an atmosphere of argon in a small Schlenk flask. The solution was sparged for ca. 15 min with argon to ensure the absence of oxygen. [Cu(MeCN)<sub>4</sub>]PF<sub>6</sub> (112 mg, 0.30 mmol, 1.00 equiv.) was added and the obtained colourless solution was stirred for ca. 15 min. The solvent was removed in vacuo and the complex was obtained quantitatively after drying in vacuo as an air-sensitive white powder. <sup>1</sup>H NMR (300 MHz, CHCl<sub>3</sub>):  $\delta$  = 4.20 (s, 4 H, oxazoline-CH<sub>2</sub>), 3.47 (s, 2 H, bridging-CH<sub>2</sub>), 2.34 (s, 3 H, MeCN), 1.41 (s, 12 H, BOX-CH<sub>3</sub>) ppm. <sup>13</sup>C{<sup>1</sup>H} NMR (75 MHz, CDCl<sub>3</sub>):  $\delta$  = 79.7 (oxazoline-CH<sub>2</sub>), 67.8 (CMe<sub>2</sub>), 28.3 (Me), 26.6 (bridging-CH<sub>2</sub>), 2.8 (MeCN) ppm, C=N and MeCN were not observed. <sup>31</sup>P NMR (121 MHz, CDCl<sub>3</sub>):  $\delta$  = −145 (sept, <sup>1</sup>J<sub>PF</sub> = 714 Hz, PF<sub>6</sub>) ppm. <sup>19</sup>F NMR (282 MHz, CDCl<sub>3</sub>):  $\delta$  = −73 (d, <sup>1</sup>J<sub>FP</sub> = 713 Hz, PF<sub>6</sub>) ppm. UV/Vis (THF): no absorbance (300–800 nm).

**[<sup>Me,H</sup>BOX-Me<sub>2</sub>)Cu(MeCN)]PF<sub>6</sub> (Cu<sup>Me</sup>):** The complex was prepared in situ and not isolated. UV/Vis (THF): no absorbance (300–800 nm).

**Preparation and Isolation of [(THF)(<sup>t</sup>Bu,<sup>H</sup>BOX-Me<sub>2</sub>)Cu]<sub>2</sub>(O<sub>2</sub><sup>2-</sup>)(PF<sub>6</sub>)<sub>2</sub> (<sup>t</sup>BuP):** <sup>t</sup>Bu,<sup>H</sup>BOX-Me<sub>2</sub> (67 mg, 0.25 mmol) was dissolved in anhydrous THF (50 mL) in a Schlenk flask and degassed by bubbling with argon to make a 5.0 mm solution. [Cu(MeCN)<sub>4</sub>](PF<sub>6</sub>) (93 mg, 0.26 mmol, 1.0 equiv.) was added and a second Schlenk flask, filled with dry O<sub>2</sub> was linked to the first flask through a short glass adapter filled with glass-wool or through a glass frit. The solution was then cooled to −78 °C and the apparatus was transferred to a freezer and stored at −82 °C. Upon slow diffusion of O<sub>2</sub> into the copper(I) complex solution, a violet precipitate (cf. Figure S3) appeared. The colourless supernatant was carefully removed by using a stainless steel syringe needle under an argon atmosphere and the residue was thoroughly washed with anhydrous diethyl ether; this was repeated three times. The residue was carefully dried for a short period in vacuo to yield <sup>t</sup>BuP (86 mg, 61%) as a very fine violet powder. The powder could be warmed to room temperature, without any problems with respect to decomposition, over at least some hours, and could be stored in air at −80 °C for at least several months. C<sub>38</sub>H<sub>68</sub>Cu<sub>2</sub>F<sub>12</sub>N<sub>4</sub>O<sub>8</sub>P<sub>2</sub>: calcd. C 40.53, H 6.09, N 4.98; found C 40.52, H 6.13, N 4.91. UV/Vis (THF, −78 °C):  $\lambda_{\text{max}}$  ( $\epsilon$ , M<sup>−1</sup>cm<sup>−1</sup>) = 333 (48 000), 500 (2100) nm. UV/Vis (powder; diffuse reflection, r. t.):  $\lambda_{\text{max}}$  = 263, 334, 520, ca. 620 *sh* nm. RR (powder, r.t.,  $\lambda_{\text{ex}}$  = 632.8 nm, selected peaks):  $\tilde{\nu}$  = 1657 ( $\nu$ {C=N}), 745 ( $\nu$ <sub>s</sub>{PF<sub>6</sub>}), 731 ( $\nu$ {O–O}), 279 ( $\nu$ {Cu–Cu}) cm<sup>−1</sup>. IR (KBr, r.t.):  $\tilde{\nu}$  = 2975 (s,  $\nu$ {C–H}), 2940 (m,  $\nu$ {C–H}), 2880 (m,  $\nu$ {C–H}), 1650 (vs,  $\nu$ {C=N}), 1475 (m), 1566 (m), 1438 (s), 1407 (w), 1388 (m), 1374 (m), 1324 (m), 1283 (w), 1259 (w), 1198 (s), 1179 (s), 1161 (m), 1063 (s), 1051 (m), 1030 (w), 1017 (w), 966 (s), 840 (vs, br,  $\nu$ <sub>as</sub>{PF<sub>6</sub>}), 788 (m), 744 (m,  $\nu$ <sub>s</sub>{PF<sub>6</sub>}), 665 (w), 558 (vs, PF<sub>6</sub>), 521 (w) cm<sup>−1</sup>. IR in Nujol mull provided identical peaks.

<sup>18</sup>O<sub>2</sub> isotopic substitution was achieved by leaving <sup>18</sup>O<sub>2</sub> (20 mL, 1 atm), under an atmosphere of argon and at −82 °C, slowly diffuse into a solution of Cu<sup>t</sup>BOX in THF (5.0 mm, 10 mL, 50  $\mu$ mol). After 1 d, the colourless supernatant was removed by using a syringe

and the violet precipitate was washed with anhydrous Et<sub>2</sub>O (5 mL). After careful drying in vacuo, <sup>18</sup>O<sub>2</sub>-labelled <sup>t</sup>BuP (26 mg, 92%) was obtained. RR (powder, r.t., λ<sub>ex</sub> = 632.8 nm, selected peaks): ν̄ = 1657 (ν{C=N}), 745 (ν<sub>s</sub>{PF<sub>6</sub>}), 692 (ν{O–O}), 278 (ν{Cu–Cu}) cm<sup>-1</sup>.

**Preparation and Isolation of [(THF)(<sup>H,H</sup>BOX-Me<sub>2</sub>)Cu]<sub>2</sub>(O<sub>2</sub><sup>2-</sup>)(PF<sub>6</sub>)<sub>2</sub> (<sup>H</sup>P):** <sup>H,H</sup>BOX-Me<sub>2</sub> (53 mg, 0.25 mmol) was dissolved in anhydrous THF (50 mL) and the solution was sparged with argon for 30 min. [Cu(MeCN)<sub>4</sub>PF<sub>6</sub>] (93 mg, 0.25 mmol, 1.00 equiv.) was added and the mixture was stirred until full dissolution. The solution was cooled to -78 °C and O<sub>2</sub> gas was generously injected. The solution turned slowly deep violet, and was stirred for 14 h. The colourless supernatant was carefully removed by using a stainless steel needle and the fine violet precipitate was washed with Et<sub>2</sub>O (2 × 10 mL). The residue was suspended in a small amount of Et<sub>2</sub>O and the suspension was transferred to a small flask. The supernatant was removed and the residue was carefully dried in vacuo for a short period. The complex (96 mg 95 μmol, 76%) was stored at -80 °C without any sign of decomposition as very fine, deep-pink powder. C<sub>30</sub>H<sub>52</sub>Cu<sub>2</sub>F<sub>12</sub>N<sub>4</sub>O<sub>8</sub>P<sub>2</sub>: calcd. C 35.54, H 5.17, N 5.53; found C 34.97, H 5.09, N 5.38. UV/Vis (THF, -78 °C): λ<sub>max</sub> (ε, M<sup>-1</sup>cm<sup>-1</sup>) = 330 (> 30 000), 504 (> 800) nm. UV/Vis (powder, diffuse reflection, r.t.): λ<sub>max</sub> = 271, 332, 512, ca. 620 (sh) nm. RR (powder, r.t., λ<sub>ex</sub> = 632.8 nm, selected peaks): ν̄ = 745 (ν<sub>s</sub> PF<sub>6</sub>), 742 (ν{O–O}), 282 (ν{Cu–Cu}) cm<sup>-1</sup>.

<sup>18</sup>O<sub>2</sub> isotopic substitution was achieved in an analogous reaction; but divergently, <sup>18</sup>O<sub>2</sub> gas (10 mL, 1 atm) in argon was allowed to diffuse slowly into the Cu<sup>H</sup>/THF solution from a second Schlenk flask through a bent glass joint at -80 °C, yield 38 mg (37 μmol, 30%); very fine, deep-pink powder. RR (powder, r.t., λ<sub>ex</sub> = 632.8 nm, selected peaks): ν̄ = 745 (ν<sub>s</sub> PF<sub>6</sub>), 703 (ν{<sup>18</sup>O–<sup>18</sup>O}), 282 (ν{Cu–Cu}) cm<sup>-1</sup>.

**Preparation of [(<sup>Me,H</sup>BOX-Me<sub>2</sub>)Cu]<sub>2</sub>(O<sub>2</sub><sup>2-</sup>)(PF<sub>6</sub>)<sub>2</sub> (<sup>Me</sup>P):** The complex was prepared from <sup>Me,H</sup>BOX-Me<sub>2</sub> (56 mg, 0.25 mmol) and [Cu(MeCN)<sub>4</sub>PF<sub>6</sub>] (93 mg, 0.25 mmol), by following the method used for <sup>t</sup>BuP. However, the complex was found to decompose partly during isolation, yield 68 mg; very fine, pink to grey powder. C<sub>24</sub>H<sub>40</sub>Cu<sub>2</sub>F<sub>12</sub>N<sub>4</sub>O<sub>6</sub>P<sub>2</sub> clacd. C 32.11, H 4.49, N 6.24; found C 32.01, H 4.67, N 5.54. UV/Vis (THF, -78 °C): λ<sub>max</sub> (ε, M<sup>-1</sup>cm<sup>-1</sup>) = 333 (> 22 000), 496 (> 500) nm. UV/Vis (powder, diffuse reflection, r.t.): λ<sub>max</sub> = 261, 331, 493, ca. 600 nm. RR (powder, r.t., λ<sub>ex</sub> = 632.8 nm, selected peaks): ν̄ = 745 (ν<sub>s</sub> PF<sub>6</sub>), 735 (ν{O–O}), 282 (ν{Cu–Cu}) cm<sup>-1</sup>.

**Thermal Degradation of <sup>t</sup>BuP and Preparation of [L(<sup>t</sup>Bu,HBOX-Me<sub>2</sub>)Cu(μ-OH)]<sub>2</sub>(PF<sub>6</sub>)<sub>2</sub>:** Storage of powdered <sup>t</sup>BuP at room temp. led slowly to a colour change from intense violet to a light-blue, which was indicative of degradation of the peroxo complex and formation of the corresponding bis(μ-hydroxo)dicopper(II) complex. Correspondingly, solutions turned slightly blue at room temperature.

**[(THF)<sub>0.85</sub>(MeCN)<sub>0.15</sub>(<sup>t</sup>Bu,HBOX-Me<sub>2</sub>)Cu(μ-OH)]<sub>2</sub>(PF<sub>6</sub>)<sub>2</sub>:** A solution of <sup>t</sup>BuP in THF at -78 °C was warmed to r.t., which was accompanied by decolouration. Under an atmosphere of argon, a small number of turquoise crystals grew from this solution after a few days, which were suitable for X-ray crystal structure determination. MS (ESI<sup>-</sup>, MeCN): *m/z* (%) = 145 (100) [PF<sub>6</sub>]<sup>-</sup>. HRMS (ESI<sup>+</sup>, MeCN): *m/z* (%) = 837.2287 (3) [(BOX)<sub>2</sub>Cu<sub>2</sub>(OH)<sub>2</sub>PF<sub>6</sub>]<sup>+</sup>; C<sub>30</sub>H<sub>54</sub>Cu<sub>2</sub>F<sub>6</sub>N<sub>4</sub>O<sub>6</sub>P requires 837.2272), 346.1313 (100) [(BOX)-Cu(OH)]<sup>+</sup>; C<sub>15</sub>H<sub>27</sub>CuN<sub>2</sub>O<sub>3</sub> requires 346.1312), 329.1285 (83) [(BOX)Cu]<sup>+</sup>; C<sub>15</sub>H<sub>26</sub>CuN<sub>2</sub>O<sub>2</sub> requires 329.1284). IR (Nujol mull, selected peaks): ν̄ = 3648 (m, ν{O–H}), 3579 (m, ν{O–H}), 2264 (w, ν<sub>MeCN}{C≡N}), 1650 (vs, ν{C=N}), 839 (vs, br, ν<sub>as}{PF<sub>6</sub>}), 742 (m, ν<sub>s}{PF<sub>6</sub>}), 557 (vs, PF<sub>6</sub>) cm<sup>-1</sup>.</sub></sub></sub>

**[(H<sub>2</sub>O)(<sup>t</sup>Bu,HBOX-Me<sub>2</sub>)Cu(μ-OH)]<sub>2</sub>(PF<sub>6</sub>)<sub>2</sub>:** Powder of <sup>t</sup>BuP was dissolved in chloroform at room temperature. From this solution, a small number of turquoise crystals crystallised by slow concentration in air. A crystal that was suitable for X-ray diffraction analysis was obtained from this solution. C<sub>30</sub>H<sub>58</sub>Cu<sub>2</sub>F<sub>12</sub>N<sub>4</sub>O<sub>8</sub>P<sub>2</sub>·3H<sub>2</sub>O calcd. C 33.55, H 6.01, N 5.22; found C 33.64, H 5.40, N 5.20. IR (Nujol mull, selected peaks): ν̄ = 3649 (w, ν{O–H}), 3583 (w, ν{O–H}), 1654 (m, ν{C=N}), 844 (s, vs, br, ν<sub>as}{PF<sub>6</sub>}), 741 (m, ν<sub>s}{PF<sub>6</sub>}), 558 (vs, PF<sub>6</sub>) cm<sup>-1</sup>.</sub></sub>

**Thermal Degradation of <sup>H</sup>P:** <sup>H</sup>P (30 mg, 26 μmol) was dissolved in CH<sub>2</sub>Cl<sub>2</sub> (10 mL) at room temp. The solution turned red and, after some minutes, green. The solution was stirred overnight, then 5% NH<sub>4</sub>OH solution (20 mL) was added and the mixture was vigorously stirred for several minutes. The aqueous phase turned slowly blue and was discarded. This was repeated two times. The organic phase was separated and washed with H<sub>2</sub>O (2 × 20 mL) and dried with Na<sub>2</sub>SO<sub>4</sub>. The solvent was removed to obtain a small amount of residue. The residue was extracted with a small amount of CDCl<sub>3</sub> and the solution was filtered. MS (ESI<sup>+</sup>, MeCN): *m/z* (%) = 225.1 (100) [(<sup>O</sup>BOX-Me<sub>2</sub> + H)]<sup>+</sup>. <sup>1</sup>H NMR (300 MHz, CDCl<sub>3</sub>): δ = 3.97 (s, 4 H, CH<sub>2</sub>), 1.29 (s, 12 H, Me) ppm. <sup>13</sup>C{<sup>1</sup>H} NMR (75.5 MHz, CDCl<sub>3</sub>): δ = 79.4 (CH<sub>2</sub>), 68.5 (CMe<sub>2</sub>), 28.0 (Me) ppm, C=N and C=O could not be observed. <sup>15</sup>N (30.4 MHz): δ = -220.5 (C=N) ppm.

**Reactivity of <sup>t</sup>BuP Towards 2,4-Di-*tert*-butylphenol (DTBP):** Anhydrous THF (8.0 mL) was cooled to -78 °C and the solution was saturated with dioxygen by injection over a period of 10 min. A 5.0 mM solution of Cu<sup>t</sup>Bu in THF (2.0 mL) was slowly injected into the cool solution; slow formation of <sup>t</sup>BuP (0.5 mM) was evident by the slow change from colourless to intense violet. After stirring for 15 min, triethylamine (10 equiv., 7.0 μL, 50 μmol) was added, followed by the addition of DTBP in fivefold excess (25 μmol). The solution was stirred at -78 °C for 16 h, along with slow warming of the cooling bath to room temperature. No change in colour of the solution was evident after some hours at -78 °C. The solvent was removed in vacuo and the residue was redissolved in dichloromethane (5 mL). HCl solution (6 M, 5 mL) was added, the phases were separated and the aqueous phase was extracted with dichloromethane (3 × 10 mL). The organic phases were combined and the volatiles were removed in vacuo. The residue was dried in vacuo and analysed by NMR spectroscopy. The residue contained the unchanged phenol (62%), and 38% was converted into the C–C coupling product 3,3',5,5'-tetra-*tert*-butyl-2,2'-biphenol (TBBP); no 3,5-di-*tert*-butyl-*o*-quinone (DTBQ) was detected. <sup>1</sup>H NMR (300 MHz, CDCl<sub>3</sub>): δ = 7.38 (d, *J* = 2.3 Hz, 2 H, Ar<sub>TBBP</sub>), 7.26 (d, *J* = 2.5 Hz, 1 H, Ar<sub>DTBP</sub>), 7.10 (d, *J* = 2.5 Hz, 2 H, Ar<sub>TBBP</sub>), 7.04 (dd, *J* = 8.1, 2.1 Hz, 1 H, Ar<sub>DTBP</sub>), 6.75 (d, *J* = 8.2 Hz, 1 H, Ar<sub>DTBP</sub>), 1.44 (s, 18 H, *t*Bu<sub>TBBP</sub>), 1.40 (s, 9 H, *t*Bu<sub>DTBP</sub>), 1.31 (s, 18 H, *t*Bu<sub>TBBP</sub>), 1.28 (s, 9 H, *t*Bu<sub>DTBP</sub>) ppm.

**Beer's Law Plots for <sup>t</sup>BuP:** Solutions of varying concentrations of <sup>t</sup>BuP (0.1–0.3 mM) in THF were prepared by injection of Cu<sup>t</sup>Bu solutions into chilled, saturated solutions of O<sub>2</sub> in THF in a dry ice/acetone bath; stock solutions of Cu<sup>t</sup>Bu (2 and 5 mM) were used. The solutions slowly became purple, and the development of the full spectrum (250–700 nm) was monitored with a 0.1 cm path length immersion probe until no change was observed. The slopes of the absorbances at 333 and 500 nm versus concentration of <sup>t</sup>BuP give extinction coefficients of approximately 48 000 and 2 100 M<sup>-1</sup>cm<sup>-1</sup>, respectively. These values are not corrected for the ca. 10% solvent contraction from room temp. to -78 °C. Concentrations of 0.3 mM or higher caused precipitation of <sup>t</sup>BuP over the short or long term.

**Reversibility of O<sub>2</sub> Activation by <sup>t</sup>BuP:** A solution of <sup>t</sup>BuP was prepared as described above by the O<sub>2</sub> injection method in an acetone/dry ice bath at –78 °C; its formation was monitored by UV/Vis spectroscopic analysis. Excess O<sub>2</sub> was then removed by several vacuum/argon cycles. The flask was warmed to –15 °C by using an ethylene glycol/dry ice bath. Reoxygenation was achieved by additional exchange of cooling baths and repeated injection of O<sub>2</sub>.

**Electrochemical Measurements:** Cyclic voltammetry (CV) and squarewave voltammetry (SWV) were conducted with Cu<sup>1/2</sup>Bu in a 0.1 M solution of tetrabutylammonium hexafluorophosphate (TBAHP, [NBu<sub>4</sub>]PF<sub>6</sub>; electrochemical grade) as the supporting electrolyte in MeCN solution. Measurements were performed at room temp. with a potentiostat/galvanostat Perkin–Elmer Model 263A, controlled by Electrochemistry Power Suite software. A glassy carbon electrode (milli-GC) was used as the working electrode, platinum as counter electrode and silver as reference electrode. All solutions were deoxygenated by bubbling with argon and measurements were performed under anaerobic conditions. The decamethylferrocene/ferrocenium couple, [Fe(Cp\*)<sub>2</sub>]<sup>+1/0</sup> {E<sub>1/2</sub> = –0.59 V vs. ferrocene, [Fe(Cp)<sub>2</sub>]<sup>+1/0</sup>, in MeCN}<sup>[68,69]</sup> was added after the measurements as the internal standard, to avoid the potential overlap of the Fe(Cp)<sub>2</sub> redox signal with other edox processes. The potential was finally converted into E vs. SCE (saturated calomel electrode) by adding 0.40 V.

**Cryo-Stopped-Flow Kinetics:** Measurements were performed with a single mixing BioLogic Science Instruments μSFM-20 Stopped-Flow Module with two syringes, controlled by a BioLogic MPS-20 Microprocessor Unit. Temperature was regulated with a Huber CC 75 cryostat with the observation head immersed into the cryosolvent (DW-Therm, DWS Synthesetechnik). The observation head was connected by an umbilical link to the μSFM-20. Spectra were recorded with an optical fibre-mounted photodiode array spectrophotometer J & M Analytik AG TIDAS. The temperature in the observation head was observed with an internal probe. The assembly was controlled with Bio-Kine32 software. The stopped-flow apparatus was flushed with argon-saturated THF to ensure the absence of air. Saturated solutions of O<sub>2</sub> in THF were prepared by bubbling dry O<sub>2</sub> gas through anhydrous THF for ca. 15 min. The solubility of O<sub>2</sub> in THF at 25 °C and 1 atm is reported to be 10.0 mM (molar fraction  $\chi = 8.16 \times 10^{-4}$ ),<sup>[70]</sup> this value was used in the calculation of the O<sub>2</sub> concentrations. Since the system was closed and the solutions had no contact to the gas phase, no change in concentration was evident. No correction for the temperature contraction of the solvent was applied. The reaction kinetic profiles were deconvoluted with the SPECFIT/32 global analysis software. Pseudo-first-order rate constants *k*<sub>obs</sub> were obtained from nonlinear regression of spectral traces with single exponential function using OriginLab OriginPro 8.5.1 software. The *k*<sub>on</sub> and *k*<sub>off</sub> values were obtained from a linear regression of a plot of *k*<sub>obs</sub> vs. O<sub>2</sub> concentration. Activation and equilibrium parameters were obtained from linear regressions of the respective Eyring and van't Hoff plots using instrumental weighted fitting with OriginPro.

**Temperature-Dependent Magnetic Susceptibility:** Measurements were carried out with a Quantum Design MPMS-XL-5 superconducting quantum interference device (SQUID) magnetometer equipped with a 5 Tesla magnet in the temperature range from 295 to 2 K. The powder sample was contained in a Teflon bucket and fixed in a nonmagnetic sample holder. Each raw data file for the measured magnetic moment was corrected for the diamagnetic contribution of the sample holder and the Teflon bucket. The molar susceptibility data was corrected for the diamagnetic contribution. Simulation of the experimental data with full-matrix diagonali-

sation of exchange coupling and Zeeman splitting was performed with the julX program.<sup>[71]</sup> Temperature-independent paramagnetism (TIP) and a Curie-behaved paramagnetic impurity (PI) with spin *S* = 1/2 were included according to  $\chi_{\text{calcd.}} = \chi \cdot (1 - PI) + \chi_{\text{mono}} \cdot PI + TIP$ . The coupling constant *J* is related to the Heisenberg–Dirac–van-Vleck Hamiltonian in the form of  $H = -2J \cdot S_1 \cdot S_2$ .

**X-ray Absorption Spectroscopy (XAS, XANES, EXAFS):** Measurements were performed at the XAS beamline of the ANKA synchrotron (Karlsruhe, Germany) under ambient conditions at 293 K. A Si(111) double crystal monochromator was used for measurements at the Cu *K*-edge (8.979 keV). The second monochromator crystal was tilted for optimal harmonic rejection. The spectra were recorded in transmission mode with ionisation chambers filled with nitrogen. The individual pressures were adjusted to optimise the signal to noise ratio. Energy calibration was performed with a copper metal foil. The solid samples were embedded in an oxygen-free boron nitride matrix and pressed into pellets. Data evaluation started with background absorption removal from the experimental absorption spectrum by subtracting a Victoreen-type polynomial.<sup>[72,73]</sup> To determine the smooth part of the spectrum, corrected for pre-edge absorption, a piecewise polynomial was used. It was adjusted in such a way that the low-*R* components of the resulting Fourier transform were minimal. After division of the background-subtracted spectrum by its smooth part, the photon energy was converted into photoelectron wavenumbers *k*. The resulting  $\chi(k)$ -function was weighted with *k*<sup>3</sup> and Fourier transformed using a Hanning window function. Data analysis was performed in *k*-space on unfiltered data. Adjustment of the common theoretical EXAFS expression

$$\chi(k) = \sum_j \frac{N_j}{kr_j^2} S_0^2(k) F_j(k) e^{-2k^2\sigma_j^2} e^{-\frac{2r_j}{\lambda}} \sin[2kr_j + \delta_j(k)]$$

(*N*<sub>*j*</sub>: one type of neighbour atoms *j* in a shell, *r*<sub>*j*</sub>: distance of atoms *j* from the X-ray absorbing atom, *S*<sub>0</sub><sup>2</sup>: amplitude reduction factor, *F*<sub>*j*</sub>: backscattering amplitude,  $\sigma^2$ : Debye–Waller like factor,  $\delta_j$ : overall phaseshift) according to the curved wave formalism of the EXCURV98 program with XALPHA phase and amplitude functions<sup>[74]</sup> yielded the structural parameters given in Table 4. The mean free path of the scattered electrons was calculated from the imaginary part of the potential (VPI set to –4.00 eV). Since an amplitude reduction factor was used to account for inelastic processes,<sup>[75]</sup> it was determined experimentally from the reference compounds Cu<sub>2</sub>O, CuO and Cu(OH)<sub>2</sub> to be 0.8 ± 0.1 by setting the coordination numbers to the crystallographic values.<sup>[76–78]</sup> An inner potential correction *E*<sub>*f*</sub> was introduced when fitting experimental data with theoretical models, which accounts for an overall phase shift between the experimental and calculated spectra. In the fitting procedure, it was taken into account that the number of fitted parameters (*N*<sub>para</sub>) did not exceed the degrees of freedom (*N*<sub>ind</sub>) that are calculated according to  $N_{\text{ind}} = (2\Delta k\Delta R/\pi)$ .<sup>[79]</sup> The quality of fit is given in terms of the *R*-factor according to:<sup>[80]</sup>

$$R = \sum_j \frac{k^3 \left| \chi^{\text{exp}}(k_j) - \chi^{\text{theo}}(k_j) \right|}{k^3 \left| \chi^{\text{exp}}(k_j) \right|} \cdot 100 \%$$

**X-ray Crystallography:** X-ray data were collected with a STOE IPDS II diffractometer (graphite monochromated Mo-*K*<sub>α</sub> radiation,  $\lambda = 0.71073$  Å) by use of  $\omega$  scans at –140 °C (Table 6). The structures were solved by direct methods (SHELXS-97) and refined on *F*<sup>2</sup> by using all reflections with SHELXL-97.<sup>[81]</sup> All non-hydrogen atoms were refined anisotropically. Most hydrogen atoms were placed in calculated positions and assigned to an isotropic

Table 6. Crystallographic data, data collection and refinement details.

	Cu <sup>I</sup> tBu	[(THF) <sub>0.85</sub> (MeCN) <sub>0.15</sub> ( <sup>t</sup> Bu,HBOX-Me <sub>2</sub> )-Cu(OH)] <sub>2</sub> (PF <sub>6</sub> ) <sub>2</sub>	[(H <sub>2</sub> O)( <sup>t</sup> Bu,HBOX-Me <sub>2</sub> )-Cu(OH)] <sub>2</sub> (PF <sub>6</sub> ) <sub>2</sub>
Empirical formula	C <sub>17</sub> H <sub>29</sub> CuF <sub>6</sub> N <sub>3</sub> O <sub>2</sub> P	C <sub>37.40</sub> H <sub>66.50</sub> Cu <sub>2</sub> F <sub>12</sub> N <sub>4.30</sub> O <sub>7.70</sub> P <sub>2</sub>	C <sub>30</sub> H <sub>56</sub> Cu <sub>2</sub> F <sub>12</sub> N <sub>4</sub> O <sub>8</sub> P <sub>2</sub>
Formula weight	515.94	1116.67	1017.81
Crystal size [mm <sup>3</sup> ]	0.34 × 0.25 × 0.14	0.34 × 0.14 × 0.10	0.27 × 0.19 × 0.11
Crystal system	monoclinic	monoclinic	monoclinic
Space group	C2/c	P2 <sub>1</sub> /c	P2 <sub>1</sub> /n
<i>a</i> [Å]	15.8795(5)	9.1739(6)	10.3550(4)
<i>b</i> [Å]	23.5320(6)	12.6410(6)	19.2516(9)
<i>c</i> [Å]	13.7259(4)	20.4258(13)	11.2821(5)
$\beta$ [°]	115.655(2)	95.710(5)	107.678(3)
<i>V</i> [Å <sup>3</sup> ]	4623.4(2)	2357.0(2)	2142.88(16)
<i>Z</i>	8	2	2
$\rho$ [g/cm <sup>3</sup> ]	1.482	1.573	1.577
<i>F</i> (000)	2128	1157	1048
$\mu$ [mm <sup>-1</sup> ]	1.079	1.070	1.168
<i>T</i> <sub>min</sub> / <i>T</i> <sub>max</sub>	0.6659/0.8790	0.7106/0.8113	0.7182/0.9103
$\theta$ range [°]	1.67–26.75	1.90–25.67	2.12–26.89
<i>hkl</i> range	±20, ±29, ±17	±11, ±15, ±24	–13 – 12, ±24, ±14
Measured refl.	27955	28616	27374
Unique refl. [ <i>R</i> <sub>int</sub> ]	4898 [0.0571]	4462 [0.0440]	4572 [0.0456]
Observed refl. [ <i>I</i> > 2σ( <i>I</i> )]	4133	3780	3826
Data/restraints/param.	4898/164/386	4462/76/347	4572/2/275
Goodness-of-fit ( <i>F</i> <sup>2</sup> )	1.022	1.039	1.062
<i>R</i> 1 [ <i>I</i> > 2σ( <i>I</i> )]	0.0355, 0.0882	0.0412, 0.1085	0.0452, 0.1021
<i>wR</i> 2 (all data)	0.0457, 0.0925	0.0517, 0.1135	0.0590, 0.1081
Resid. el. dens. [e/Å <sup>3</sup> ]	–0.281/0.437	–0.347/0.628	–0.569/0.740

displacement parameter of 1.2/1.5 *U*<sub>eq</sub>(C). The oxygen-bound hydrogen atoms in [(H<sub>2</sub>O)(<sup>t</sup>Bu,HBOX-Me<sub>2</sub>)Cu(OH)]<sub>2</sub>(PF<sub>6</sub>)<sub>2</sub> were refined with a fixed isotropic displacement parameter of 0.08 Å<sup>2</sup> and DFIX restraints for the O–H distances of 0.82 Å. Face-indexed absorption corrections were performed numerically with the program X-RED.<sup>[82]</sup> In Cu<sup>I</sup>tBu and [(THF)<sub>0.85</sub>(MeCN)<sub>0.15</sub>(<sup>t</sup>Bu,HBOX-Me<sub>2</sub>)-Cu(OH)]<sub>2</sub>(PF<sub>6</sub>)<sub>2</sub> the PF<sub>6</sub><sup>–</sup> counterions were found to be disordered as well as parts of the ligand in case of the former and for the coordinating solvent molecules in case of the latter compound. The disorder of the two different solvent molecules in the latter case is related to the disorder of the counterion. After the initial refinement, the occupancy factors were fixed at 0.85 and 0.15, which represent the fraction of the two solvents (THF and MeCN) and the occupancy of the PF<sub>6</sub><sup>–</sup> with respect to two alternate positions. EADP constraints and DELU, SIMU and BUMP restraints were applied to model the disorder. Two counterions (occupancy 0.5) in Cu<sup>I</sup>tBu were found to be disordered about twofold axes. Additionally parts of the ligands are disordered [O2, C8, C9, C10, C11; occupancy factors: 0.584(11)/0.416(11)]. SADI, SIMU and DELU restraints were used to model the disorder.

CCDC-978251 (Cu<sup>I</sup>tBu), -978252 {[(THF)<sub>0.85</sub>(MeCN)<sub>0.15</sub>(<sup>t</sup>Bu,HBOX-Me<sub>2</sub>)Cu(OH)]<sub>2</sub>(PF<sub>6</sub>)<sub>2</sub>} and -978253 {[(H<sub>2</sub>O)(<sup>t</sup>Bu,HBOX-Me<sub>2</sub>)Cu(OH)]<sub>2</sub>(PF<sub>6</sub>)<sub>2</sub>} contain the supplementary crystallographic data for this paper. These data can be obtained free of charge from The Cambridge Crystallographic Data Centre via [http://www.ccdc.cam.ac.uk/data\\_request/cif](http://www.ccdc.cam.ac.uk/data_request/cif).

**Theoretical Calculations:** Density functional theory (DFT) calculations were performed with the ORCA 2.9.1 electronic structure program package by F. Neese.<sup>[83]</sup> The geometry of {[(<sup>t</sup>Bu,HBOX-Me<sub>2</sub>)-Cu]<sub>2</sub>(O<sub>2</sub>)(MeCN)<sub>2</sub>}<sup>2+</sup> was fully optimised starting from coordinates obtained from the X-ray crystal structure of [(MeCN)<sub>2</sub>{(<sup>t</sup>Bu,HBOX-Me<sub>2</sub>)Cu]<sub>2</sub>(OH)<sub>2</sub>}<sup>2+</sup> after manipulation of the Cu<sub>2</sub>O<sub>2</sub> distances (using the molecule editor Avogadro 1.1.0<sup>[84]</sup>). Ligand geometries were used without truncation. Geometry optimisations and single-point calculations were performed by using Becke's three-param-

eter hybrid functional with the correlation functional of Lee, Yang, and Parr (B3LYP).<sup>[85,86]</sup> The valence triple- $\zeta$  plus polarisation basis sets (def2-TZVPP)<sup>[87,88]</sup> were used on copper, oxygen and nitrogen atoms and double- $\zeta$  split valence polarisation sets (def2-SVP)<sup>[87,89]</sup> on carbon and hydrogen, as implemented in ORCA. The resolution of identity/chain of spheres exchange approximation (RIJCOSX),<sup>[90–92]</sup> together with the matching def2-TZVPP/J and def2-SVP/J auxiliary basis set were used to accelerate the calculations. Default convergence criteria were used for geometry optimisation calculations (OPT); for SCF calculations, strict convergence criteria were used (TightSCF). Slow convergence was expected (SlowConv). Solvent effects were considered in all calculations by invoking the conductor-like screening model (COSMO) with the selection of THF as a solvent. A DFT spin-unrestricted formalism (UKS) has been applied to first calculate a high-spin triplet state (*S* = 1) geometry, which was then used to calculate the spin-polarised broken-symmetry (BS) solution.<sup>[55,56]</sup> Therefore, the spin on one copper atom was flipped by invoking the “FlipSpin” mechanism in ORCA in expectation of an antiferromagnetically coupled state, *M*<sub>S</sub> = 0 (FinalMs 0). Time-dependent DFT (TD-DFT) calculations and natural transition orbital (NTO) analysis were undertaken with ORCA version 3.0.1. Calculations on the geometry-optimised coordinates were performed using the B3LYP functional together with basis sets and COSMO model stated above. The first 16 excited states were calculated; the maximum dimension of the expansion space in the Davidson procedure (MaxDim) was 320. Absorption spectra were created by the utility program ‘orca\_mapspc’ and plotted with the program package OriginLab OriginPro 8.5.0G. Molecular structures, orbitals and spin densities were visualised with the UCSF Chimera package.<sup>[93]</sup>

**Supporting Information** (see footnote on the first page of this article): Details of electrochemical experiments, DFT calculations and kinetic measurements. Further vibrational spectra, UV/Vis spectra and traces, Beer's law plot, HRMS (ESI) spectra of Cu<sub>2</sub>(OH)<sub>2</sub> and van-der-Waals plots of X-ray structures.

## Acknowledgments

This work has been carried out in the framework of the International PhD program CaSuS (see www.casus.uni-goettingen.de) and the European COST program CM 1003. The Karlsruhe synchrotron ANKA (Germany) and Dr. Stefan Mangold are acknowledged for providing beamtime and help for the XAS measurements.

- [1] L. M. Mirica, X. Ottenwaelder, T. D. P. Stack, *Chem. Rev.* **2004**, *104*, 1013–1045.
- [2] E. A. Lewis, W. B. Tolman, *Chem. Rev.* **2004**, *104*, 1047–1076.
- [3] S. Itoh, *Curr. Opin. Chem. Biol.* **2006**, *10*, 115–122.
- [4] E. I. Solomon, D. E. Heppner, E. M. Johnston, J. W. Ginsbach, J. Cirera, M. Qayyum, M. T. Kieber-Emmons, C. H. Kjaergaard, R. G. Hadt, L. Tian, *Chem. Rev.* **2014**, *114*, 3659–3853.
- [5] K. A. Magnus, H. Ton-That, J. E. Carpenter, *Chem. Rev.* **1994**, *94*, 727–735.
- [6] K. E. van Holde, K. I. Miller, H. Decker, *J. Biol. Chem.* **2001**, *276*, 15563–15566.
- [7] Y. Matoba, T. Kumagai, A. Yamamoto, H. Yoshitsu, M. Sugiyama, *J. Biol. Chem.* **2006**, *281*, 8981–8990.
- [8] H. Decker, T. Schweikardt, F. Tuzcek, *Angew. Chem. Int. Ed.* **2006**, *45*, 4546–50; *Angew. Chem.* **2006**, *118*, 4658.
- [9] C. Gerdemann, C. Eicken, B. Krebs, *Acc. Chem. Res.* **2002**, *35*, 183–91.
- [10] E. I. Solomon, P. Chen, M. Metz, S.-K. Lee, A. E. Palmer, *Angew. Chem. Int. Ed.* **2001**, *40*, 4570–4590; *Angew. Chem.* **2001**, *113*, 4702.
- [11] H. Decker, in: *Encycl. Inorg. Chem* (Eds.: R. B. King, R. H. Crabtree, C. M. Lukehart, D. A. Atwood, R. A. Scott), John Wiley & Sons, Chichester, UK, **2006**.
- [12] N. Kitajima, K. Fujisawa, C. Fujimoto, Y. Moro-oka, S. Hashimoto, T. Kitagawa, K. Toriumi, K. Tatsumi, A. Nakamura, *J. Am. Chem. Soc.* **1992**, *114*, 1277–1291.
- [13] N. Kitajima, Y. Moro-oka, *Chem. Rev.* **1994**, *94*, 737–757.
- [14] J. A. Halfen, S. Mahapatra, E. C. Wilkinson, S. Kaderli, V. G. Young, L. Que, A. D. Zuberbühler, W. B. Tolman, *Science* **1996**, *271*, 1397–1400.
- [15] S. Mahapatra, J. Halfen, E. C. Wilkinson, G. Pan, X. Wang, V. Young Jr., C. Cramer, L. Que Jr., W. B. Tolman, *J. Am. Chem. Soc.* **1996**, *118*, 11555–11574.
- [16] R. R. Jacobson, Z. Tyeklar, A. Farooq, K. D. Karlin, S. Liu, J. Zubieta, *J. Am. Chem. Soc.* **1988**, *110*, 3690–3692.
- [17] G. Y. Park, M. F. Qayyum, J. Woertink, K. O. Hodgson, B. Hedman, A. A. Narducci Sarjeant, E. I. Solomon, K. D. Karlin, *J. Am. Chem. Soc.* **2012**, *134*, 8513–8524.
- [18] Z. Hu, R. D. Williams, D. Tran, T. G. Spiro, S. M. Gorun, *J. Am. Chem. Soc.* **2000**, *122*, 3556–3557.
- [19] M. Kodera, K. Katayama, Y. Tachi, K. Kano, S. Hirota, S. Fujinami, M. Suzuki, *J. Am. Chem. Soc.* **1999**, *121*, 11006–11007.
- [20] E. I. Solomon, J. W. Ginsbach, D. E. Heppner, M. T. Kieber-Emmons, C. H. Kjaergaard, P. J. Smeets, L. Tian, J. S. Woertink, *J. Chem. Soc. Faraday Trans.* **2011**, *148*, 11.
- [21] E. I. Solomon, *Inorg. Chem.* **2006**, *45*, 8012–25.
- [22] R. H. Holm, P. Kennepohl, E. I. Solomon, *Chem. Rev.* **1996**, *96*, 2239–2314.
- [23] M. Rolff, J. Schottenheim, H. Decker, F. Tuzcek, *Chem. Soc. Rev.* **2011**, *40*, 4077–98.
- [24] I. A. Koval, P. Gamez, C. Belle, K. Selmececi, J. Reedijk, *Chem. Soc. Rev.* **2006**, *35*, 814–840.
- [25] B. Hazes, K. A. Magnus, C. Bonaventura, J. Bonaventura, Z. Dauter, K. H. Kalk, W. G. Hol, *Prot. Sci.* **1993**, *2*, 597–619.
- [26] K. A. Magnus, B. Hazes, H. Ton-That, C. Bonaventura, J. Bonaventura, W. G. Hol, *Proteins: Struct., Funct., Bioinf.* **1994**, *19*, 302–309.
- [27] A. K. Ghosh, P. Mathivanan, J. Cappiello, *Tetrahedron: Asymmetry* **1998**, *9*, 1–45.
- [28] M. Gómez, G. Muller, M. Rocamora, *Coord. Chem. Rev.* **1999**, *193–195*, 769–835.
- [29] K. A. Jørgensen, M. Johannsen, S. Yao, H. Audrain, J. Thorhauge, *Acc. Chem. Res.* **1999**, *32*, 605–613.
- [30] J. S. Johnson, D. A. Evans, *Acc. Chem. Res.* **2000**, *33*, 325–335.
- [31] H. A. McManus, P. J. Guiry, *Chem. Rev.* **2004**, *104*, 4151–4202.
- [32] G. Desimoni, G. Faita, K. A. Jørgensen, *Chem. Rev.* **2011**, *111*, PR284–PR437.
- [33] R. Rasappan, D. Laventine, O. Reiser, *Coord. Chem. Rev.* **2008**, *252*, 702–714.
- [34] S. Dagorne, S. Bellemin-Laponnaz, A. Maise-François, *Eur. J. Inorg. Chem.* **2007**, 913–925.
- [35] A. Walli, S. Dechert, F. Meyer, *Eur. J. Org. Chem.* **2013**, 7044–7049.
- [36] M. J. Baldwin, D. E. Root, J. E. Pate, K. Fujisawa, N. Kitajima, E. I. Solomon, *J. Am. Chem. Soc.* **1992**, *114*, 10421–10431.
- [37] L. M. Mirica, M. Vance, D. J. Rudd, B. Hedman, K. O. Hodgson, E. I. Solomon, T. D. P. Stack, *J. Am. Chem. Soc.* **2002**, *124*, 9332–9333.
- [38] L. M. Mirica, M. Vance, D. J. Rudd, B. Hedman, K. O. Hodgson, E. I. Solomon, T. D. P. Stack, *Science* **2005**, *308*, 1890–1892.
- [39] L. M. Mirica, D. J. Rudd, M. A. Vance, E. I. Solomon, K. O. Hodgson, B. Hedman, T. D. P. Stack, *J. Am. Chem. Soc.* **2006**, *128*, 2654–2665.
- [40] K. E. Dalle, T. Gruene, S. Dechert, S. Demeshko, F. Meyer, *J. Am. Chem. Soc.* **2014**, *136*, 7428–7434.
- [41] M. J. Henson, V. Mahadevan, T. D. P. Stack, E. I. Solomon, *Inorg. Chem.* **2001**, *40*, 5068–5069.
- [42] K. Connors, *Chemical Kinetics: The Study of Reaction Rates, in: Solution*, VCH Publishers, New York, Weinheim, Germany, Cambridge, UK, **1990**.
- [43] S. V. Kryatov, E. V. Rybak-Akimova, S. Schindler, *Chem. Rev.* **2005**, *105*, 2175–2226.
- [44] K. D. Karlin, S. Kaderli, A. D. Zuberbühler, *Acc. Chem. Res.* **1997**, *30*, 139–147.
- [45] E. V. Rybak-Akimova, in: *Phys. Inorg. Chem. React. Process. Appl.* (Ed.: A. Bakac), John Wiley & Sons, **2011**, p. 109–188.
- [46] E. V. Rybak-Akimova, W. Otto, P. Deardorf, R. Roesner, D. H. Busch, *Inorg. Chem.* **1997**, *36*, 2746–2753.
- [47] E. V. Rybak-Akimova, K. Marek, M. Masarwa, D. H. Busch, *Inorg. Chim. Acta* **1998**, *270*, 151–161.
- [48] N. W. Aboelella, S. V. Kryatov, B. F. Gherman, W. W. Brennessel, V. G. Young Jr., R. Sarangi, E. V. Rybak-Akimova, K. O. Hodgson, B. Hedman, E. I. Solomon, C. J. Cramer, W. B. Tolman, *J. Am. Chem. Soc.* **2004**, *126*, 16896–16911.
- [49] S. V. Kryatov, E. V. Rybak-Akimova, V. L. MacMurdo, L. Que, *Inorg. Chem.* **2001**, *40*, 2220–2228.
- [50] A. Kunishita, M. Z. Ertem, Y. Okubo, T. Tano, H. Sugimoto, K. Ohkubo, N. Fujieda, S. Fukuzumi, C. J. Cramer, S. Itoh, *Inorg. Chem.* **2012**, *51*, 9465–9480.
- [51] R. Diaz-Torres, S. Alvarez, *J. Chem. Soc., Dalton Trans.* **2011**, *40*, 10742–50.
- [52] J. L. DuBois, P. Mukherjee, A. M. Collier, J. M. Mayer, E. I. Solomon, B. Hedman, T. D. P. Stack, K. O. Hodgson, *J. Am. Chem. Soc.* **1997**, *119*, 8578–8579.
- [53] J. L. DuBois, P. Mukherjee, T. D. P. Stack, B. Hedman, E. I. Solomon, K. O. Hodgson, *J. Am. Chem. Soc.* **2000**, *122*, 5775–5787.
- [54] L. S. Kau, D. J. Spira-Solomon, J. E. Penner-Hahn, K. O. Hodgson, E. I. Solomon, *J. Am. Chem. Soc.* **1987**, *109*, 6433–6442.
- [55] A. P. Ginsberg, *J. Am. Chem. Soc.* **1980**, *102*, 111–117.
- [56] L. Noodleman, C. Y. Peng, D. A. Case, J.-M. Mouesca, *Coord. Chem. Rev.* **1995**, *144*, 199–244.
- [57] E. Pidcock, H. V. Obias, M. Abe, H. Liang, K. D. Karlin, E. I. Solomon, *J. Am. Chem. Soc.* **1999**, *121*, 1299–1308.
- [58] E. I. Solomon, D. M. Dooley, R.-H. Wang, H. B. Gray, M. Cerdonio, F. Mogno, G. L. Romani, *J. Am. Chem. Soc.* **1976**, *98*, 1029–1031.

- [59] K. D. Karlin, Z. Tyeklár, A. Farooq, R. R. Jacobson, E. Sinn, D. W. Lee, J. E. Bradshaw, L. J. Wilson, *Inorg. Chim. Acta* **1991**, *182*, 1–3.
- [60] K. D. Karlin, Z. Tyeklár, A. Farooq, M. S. Haka, P. Ghosh, R. W. Cruse, Y. Gultneh, J. C. Hayes, P. J. Toscano, J. Zubieta, *Inorg. Chem.* **1992**, *31*, 1436–1451.
- [61] Y. Takano, K. Koizumi, H. Nakamura, *Inorg. Chim. Acta* **2009**, *362*, 4578–4584.
- [62] S. Herres-Pawlis, P. Verma, R. Haase, P. Kang, C. T. Lyons, E. C. Wasinger, U. Flörke, G. Henkel, T. D. P. Stack, *J. Am. Chem. Soc.* **2009**, *131*, 1154–69.
- [63] A. W. Addison, T. N. Rao, J. Reedijk, J. van Rijn, G. C. Verschoor, *J. Chem. Soc., Dalton Trans.* **1984**, 1349–1356.
- [64] S. Itoh, M. Taki, H. Nakao, P. L. Holland, W. B. Tolman, L. Que Jr., S. Fukuzumi, *Angew. Chem. Int. Ed.* **2000**, *39*, 398–400; *Angew. Chem.* **2000**, *112*, 409.
- [65] S. Yokota, Y. Tachi, S. Itoh, *Inorg. Chem.* **2002**, *41*, 1342–1344.
- [66] D. R. Burfield, R. H. Smithers, *J. Org. Chem.* **1978**, *43*, 3966–3968.
- [67] G. J. Kubas, B. Monzyk, A. L. Crumblis, *Inorg. Synth.* **1979**, *19*, 90–92.
- [68] N. G. Connelly, W. E. Geiger, *Chem. Rev.* **1996**, *96*, 887–910.
- [69] J. R. Aranzaes, M.-C. Daniel, D. Astruc, *Can. J. Chem.* **2006**, *84*, 288–299.
- [70] R. Battino, T. R. Rettich, T. Tominaga, *J. Phys. Chem. Ref. Data* **1983**, *12*, 163.
- [71] E. Bill, *JulX Simulation Program for Static Molar Magnetic Susceptibilities*, Max Planck Institute For Chemical Energy Conversion, Mülheim an der Ruhr, Germany, eckhard.bill@cec.mpg.de.
- [72] T. S. Ertel, H. Bertagnolli, S. Hückmann, U. Kolb, D. Peter, *Appl. Spectrosc.* **1992**, *46*, 690–698.
- [73] M. Newville, P. Livins, Y. Yacoby, J. Rehr, E. Stern, *Phys. Rev. B* **1993**, *47*, 14126–14131.
- [74] S. J. Gurman, N. Binsted, I. Ross, *J. Phys. C* **1984**, *17*, 143–151.
- [75] M. Roy, S. J. Gurman, *J. Synchrotron Radiat.* **1999**, *6*, 228.
- [76] A. Kirfel, K. Eichhorn, *Acta Crystallogr., Sect. A* **1990**, *46*, 271–284.
- [77] H. Yamada, Y. Soejima, X. G. Zheng, M. Kawaminami, *Trans. Mater. Res. Soc. Jpn.* **2000**, *25*, 1199–1202.
- [78] H. R. Oswald, A. Reller, H. W. Schmalke, E. Dubler, *Acta Crystallogr., Sect. C* **1990**, *46*, 2279–2284.
- [79] E. Stern, *Phys. Rev. B* **1993**, *48*, 9825–9827.
- [80] N. Binsted, *EXCURV98: CCLRC Daresbury Laboratory Computer Program, Manual*, **1998**.
- [81] G. M. Sheldrick, *Acta Crystallogr., Sect. A* **2008**, *64*, 112–122.
- [82] *X-RED*, STOE & CIE GmbH, Darmstadt (Germany), **2002**.
- [83] F. Neese, *WIREs Comput. Mol. Sci.* **2012**, *2*, 73–78.
- [84] M. D. Hanwell, D. E. Curtis, D. C. Lonie, T. Vandermeersch, E. Zurek, G. R. Hutchison, *J. Cheminf.* **2012**, *4*, 17.
- [85] A. D. Becke, *J. Chem. Phys.* **1993**, *98*, 5648–5652.
- [86] C. Lee, W. Yang, R. G. Parr, *Phys. Rev. B* **1988**, *37*, 785–789.
- [87] F. Weigend, R. Ahlrichs, *Phys. Chem. Chem. Phys.* **2005**, *7*, 3297–3305.
- [88] A. Schäfer, C. Huber, R. Ahlrichs, *J. Chem. Phys.* **1994**, *100*, 5829–5835.
- [89] A. Schäfer, H. Horn, R. Ahlrichs, *J. Chem. Phys.* **1992**, *97*, 2571–2577.
- [90] F. Neese, *J. Comput. Chem.* **2003**, *24*, 1740–1747.
- [91] F. Neese, F. Wennmohs, A. Hansen, U. Becker, *Chem. Phys.* **2009**, *356*, 98–109.
- [92] S. Kossmann, F. Neese, *Chem. Phys. Lett.* **2009**, *481*, 240–243.
- [93] E. F. Pettersen, T. D. Goddard, C. C. Huang, G. S. Couch, D. M. Greenblatt, E. C. Meng, T. E. Ferrin, *J. Comput. Chem.* **2004**, *25*, 1605–1612.

Received: May 2, 2014  
Published Online: August 1, 2014